

Stretching Response of a Polymer Chain with Deformable Bonds

Jie Zhu and Laurence Brassart

Department of Engineering Science, University of Oxford, Oxford OX1 3PJ, United Kingdom.

The stretching response of polymer chains fundamentally determines the mechanical properties of polymer networks. In this work, we develop a statistical mechanics model that incorporates both bond stretching and bond angle deformation, enabling accurate predictions of chain behavior up to large forces. This model achieves excellent agreement with experimental data for carbon chains across all force regimes using physical parameters only. We further propose a semi-analytical deformable Freely Rotating Chain (dFRC) model, which represents the chain as a freely rotating chain with effective bond stretch and bond angle that depend on the chain stretch. We show that the dFRC model is accurate over the entire force range using the same physical parameters as the statistical model without fitting. Additionally, the dFRC model provides a direct estimate of the bond force, which is crucial to predict chain scission. By capturing key bond deformations while remaining computationally efficient, our work lays the foundation for future modeling of polymer network elasticity and failure.

Models for single polymer chains under applied forces are important for understanding how molecular structure influences their stretching behavior. These models also constitute fundamental building blocks of micromechanical theories of rubber elasticity [1], which enable the prediction of polymer network properties through suitable upscaling procedures [2–6]. At low forces, the stretching response is dominated by entropic contributions, which is captured by models such as the Freely Jointed Chain (FJC) model, which represents the chain as freely jointed bonds, and the Freely Rotating Chain (FRC) model, which introduces a fixed angle between pairs of consecutive bonds [7]. However, at high forces, energetic contributions due to bond stretching and bond angle opening become significant, rendering purely entropic models inadequate [8–10]. Extendable FJC models incorporating bond stretching have been proposed [11–15], but they neglect bond angle deformation, raising questions about the physical meaning of their best-fit parameters. Similarly, extendable Worm-Like Chain (WLC) models [12, 16, 17] allow bond stretching as well as bond angle deformation, but they assume an equilibrium angle of 0° , limiting their range of application. Despite these efforts, polymer chain models that incorporate both bond stretching and bond angle deformation remain scarce [18], and the effect of their simultaneous interplay on the stretching response up to large deformations has not been thoroughly explored. Moreover, the lack of an analytical force-extension relationship for such chains hinders the development of accurate micromechanical models of polymer network elasticity and failure at large deformations.

In this letter, we address these challenges by developing a statistical mechanics model and a semi-analytical model to describe the stretching behavior of polymer chains, incorporating both bond stretching and bond angle deformation. In the statistical model, we use the transfer-matrix (TM) technique to calculate the partition function in the Gibbs ensemble, from which we obtain the

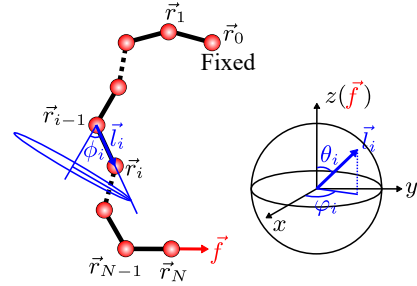


FIG. 1. A polymer chain with N bonds subjected to a constant force \vec{f} at \vec{r}_N . The other chain end at \vec{r}_0 is fixed. The orientation of each bond is described using spherical coordinates, with the z -axis aligned with the force.

Gibbs free energy and force-extension relationship. Our results show that both bond stretching and bond angle opening significantly affect the chain stiffness at large deformations. Using molecular mechanics-derived parameters without any fitting, the statistical model predicts the force-extension curve of carbon chains and shows excellent agreement with experimental data across the entire force range. To enhance computational tractability, we further develop a semi-analytical model by representing the polymer chain as a deformable FRC (dFRC) where bond length and bond angle depend on the applied chain stretch, inspiring from original ideas in Refs [15, 18]. The dFRC model is based on a new analytical formula for the classical FRC, which is shown to be valid across the entire force range. We validate the dFRC model against reference solutions obtained using the TM technique, showing excellent agreement for experimentally relevant parameters. By accurately capturing bond stretching and bond angle deformation, the dFRC model is promising for advancing micromechanical theories of rubber elasticity, particularly for describing failure by chain scission, where precise bond stretch predictions are critical.

We consider a polymer chain composed of N bonds (Fig. 1). The configuration of the chain is described

by the positions \vec{r}_i of each atom ($i = 0, \dots, N$). The chain is subjected to a prescribed force \vec{f} at the terminal atom \vec{r}_N , with the other terminal atom fixed at the origin $\vec{r}_0 = (0, 0, 0)$. Each bond vector, $\vec{l}_i = \vec{r}_i - \vec{r}_{i-1}$ ($i = 1, \dots, N$), is represented in spherical coordinates as $\vec{l}_i = l_i (\sin \theta_i \cos \varphi_i, \sin \theta_i \sin \varphi_i, \cos \theta_i)$, where l_i is the bond length, θ_i is the polar angle relative to the direction of the applied force \vec{f} , and φ_i is the azimuthal angle. The bond angle between adjacent bonds, $\phi_i = \angle(\vec{l}_{i-1}, \vec{l}_i)$, ($i = 2, \dots, N$), is calculated as $\phi_i = \arccos[\sin \theta_i \sin \theta_{i-1} \cos \omega_i + \cos \theta_i \cos \theta_{i-1}]$, where $\omega_i = \varphi_i - \varphi_{i-1}$ is the difference in azimuthal angle between two adjacent bonds.

The partition function for the chain in the Gibbs ensemble is given by (Sec. S1):

$$Z \propto \int e^{-\frac{1}{k_B T} [\sum_{i=1}^N v_{str}(l_i) + \sum_{i=2}^N v_{ben}(\phi_i) - \sum_{i=1}^N f l_i \cos \theta_i]} dq \quad (1)$$

where $q = (\vec{l}_1, \dots, \vec{l}_N)$, k_B is the Boltzmann constant, T is the temperature, and $f = \|\vec{f}\|$. The bond stretching energy is assumed quadratic for simplicity: $v_{str}(l_i) = \frac{1}{2} k_l (l_i - l_e)^2$, where l_e is the equilibrium bond length, and k_l is the bond stretching stiffness. When $k_l \rightarrow \infty$, bonds are rigid with length l_e . Similarly, the bond angle deformation energy (“bending energy”) is taken as $v_{ben}(\phi_i) = \frac{1}{2} k_\phi (\phi_i - \phi_e)^2$, where ϕ_e is the equilibrium bond angle, and k_ϕ is the bond angle deformation stiffness. When $k_\phi = 0$, bond angles are freely deformable. When $k_\phi \rightarrow \infty$, bond angles are fixed at ϕ_e . We neglect the bond rotation energy, as it is typically much smaller than the energy of bond stretching and bond angle opening in homogeneous backbone chains (e.g., chains with carbon-carbon backbone) [9], so that bonds can freely rotate.

The bending energy couples the configurations of two consecutive bonds. Consequently, the Gibbs partition function (Eq. 1) cannot be factorized into N identical terms, different from the extensible FJC model. To address this difficulty, we employ the numerical TM method [19], building on the work of Livadaru et al., who applied this technique to the classical FRC model [20]. The weighted probability density of finding the $(i+1)$ th bond at an angle θ can be expressed as (Sec. S2.1):

$$W_{i+1}(\theta) = \int P_i(\theta') T(\theta, \theta') d\theta' \quad (2)$$

where $P_i(\theta) = W_i(\theta) / [\int W_i(\theta') d\theta']$ is the bond orientation probability density of the i th bond, and $\int P_i(\theta) d\theta = 1$. The transfer operator $T(\theta, \theta')$ characterizes the interaction between the $(i+1)$ th bond at angle θ and the i th bond at angle θ' , which is given by

$$T(\theta, \theta') = \iint e^{-\frac{1}{k_B T} [v_{str}(l) + v_{ben}(\phi) - f l \cos \theta]} l^2 \sin \theta d\omega dl \quad (3)$$

where l is the length of the $(i+1)$ th bond, ϕ is the bond angle between the $(i+1)$ th and i th bonds, and ω is the difference in their azimuthal angles. The weighted probability density of the first bond is given by

$$W_1(\theta) = \iint e^{-\frac{1}{k_B T} [v_{str}(l) - f l \cos \theta]} l^2 \sin \theta d\omega dl \quad (4)$$

where ω is the azimuthal angle of the first bond. Starting with $W_1(\theta)$, the weighted probability density of each subsequent bond can be determined iteratively. Finally, the Gibbs partition function (Eq. 1) can be obtained as (Sec. S2.1)

$$Z \propto \prod_{i=1}^N \left[\int W_i(\theta) d\theta \right] \quad (5)$$

The chain end-to-end distance r is derived from the Gibbs partition function as:

$$r = k_B T \frac{\partial}{\partial f} \ln Z = -\frac{\partial G}{\partial f} \quad (6)$$

where $G = -k_B T \ln Z$ is the Gibbs free energy of the chain. Note that $r = \|\vec{r}\| = \|\langle \vec{r}_N \rangle\|$ is the norm of the thermal average of the chain end-to-end vector over fluctuations. The partition function is calculated using quadrature methods, and the force-extension relationship is obtained by numerical differentiation, see Sec. S2.1.

In the freely jointed bond limit ($k_\phi = 0$), the model reduces to the extensible FJC model, and the transfer operator simplifies to $T(\theta)$ (Sec. S2.2). In the fixed bond angle limit ($k_\phi \rightarrow \infty$), the extensible FRC model is obtained, and the transfer operator involves a Dirac delta function, $\delta(\phi - \phi_e)$, requiring special considerations (Sec. S2.3). Bond orientation probabilities for different cases are illustrated in Sec. S3, where we also show that $P_i(\theta)$ converges to a stable distribution $P_\infty(\theta)$ as the bond index i increases, corresponding to the weighted probability density $W_\infty(\theta) = \int P_\infty(\theta') T(\theta, \theta') d\theta'$. For sufficiently large N , the Gibbs partition function (Eq. 5) can be approximated as $Z \propto [\int W_\infty(\theta) d\theta]^N$, and the force-extension relationship becomes independent of N , corresponding to the thermodynamic limit. The effect of N on the force-extension relationship is further discussed in Sec. S4.1.

We examine how bond stretching and bond angle opening influence the stretching response in the thermodynamic limit ($N \rightarrow \infty$). To isolate their individual effects, we analyze the following limiting cases:

(i) Extensible bonds and freely-deformable bond angles ($k_\phi = 0$). This is the extensible FJC model. Force-extension curves are shown in Fig. 2a for different values of the normalized bond stretching stiffness, $k_l l_e^2 / k_B T$. At low forces, the chain stretching response is primarily governed by entropic elasticity and follows the Gaussian chain model $r = N l_e^2 f / (3 k_B T)$, where $N l_e^2 / (3 k_B T)$

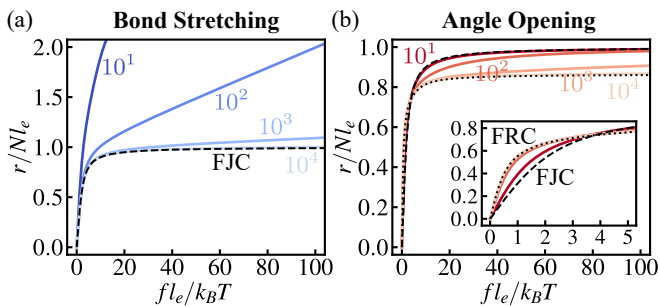


FIG. 2. Effect of bond deformation on the stretching response of polymer chains. (a) Bond stretching: force-extension curves for chains with freely jointed extensible bonds ($k_\phi = 0$; $k_l l_e^2 / k_B T = 10^1, 10^2, 10^3, 10^4$). (b) Angle opening: force-extension curves for chains with rigid bonds ($k_l l_e^2 / k_B T \rightarrow \infty$) and deformable bond angles ($\phi_e = 60^\circ$; $k_\phi \pi^2 / k_B T = 10^1, 10^2, 10^3, 10^4$).

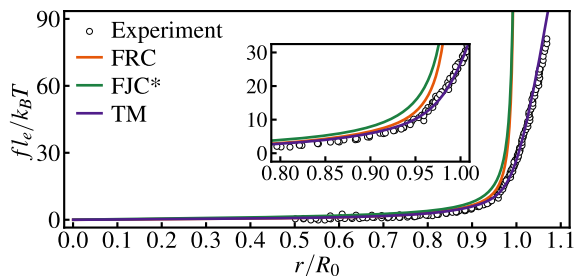


FIG. 3. Stretching response of carbon chains predicted by the statistical (TM: extensible bonds, deformable bond angles), classical FRC (rigid bonds, fixed bond angles), and equivalent FJC (FJC*: rigid Kuhn segments) models. Experimental data from [9]. R_0 denotes the contour length at zero force.

represents the entropic spring constant [21]. As the force increases, bond stretching results in a second elastic regime with stiffness proportional to k_l . In the limit $k_l l_e^2 / k_B T \rightarrow \infty$, the extensible FJC model recovers the FJC model with contour length $R_{max} = N l_e$. These results are consistent with the findings in Ref. [12].

(ii) Rigid bonds ($k_l l_e^2 / k_B T \rightarrow \infty$) and deformable bond angles. Force-extension curves are shown in Fig. 2b for different values of the normalized bond angle deformation stiffness, $k_\phi \pi^2 / k_B T$, and $\phi_e = 60^\circ$. For $k_\phi = 0$, the model recovers the FJC model. For $k_\phi \pi^2 / k_B T \rightarrow \infty$, the model tends to the FRC model with contour length $R_{max} = N l_e \cos(\phi_e/2)$. At low applied forces, increasing k_ϕ softens the chain since the coiled configuration becomes less probable. As the force increases, a larger k_ϕ stiffens the chain as it approaches its extensibility limit. This stiffening effect depends on the equilibrium bond angle ϕ_e , with a large ϕ_e leading to a reduced contour length, see Sec. S4.2.

We next use our statistical model to simulate the stretching response of polymer chains with a carbon-carbon backbone, such as polyethylene (PE), polystyrene

(PS), and polypropylene (PP). Molecular mechanics calculations indicate that these chains have an equilibrium bond length of $l_e = 1.53 \text{ \AA}$ and an equilibrium bond angle of $\phi_e = 69^\circ$, with stiffness $k_l = 4.29 \times 10^{-18} \text{ J/\AA}^2$ for bond stretching and $k_\phi = 7.47 \times 10^{-19} \text{ J/rad}^2$ for bond angle opening [22]. Using these parameters, we simulate the chain stretching response at room temperature ($T = 23^\circ$) and compare model predictions with experimental data from [9]. For comparison, we also include predictions of the FRC model, which assumes rigid bonds and fixed bond angles, and the equivalent FJC model (FJC*), which represents the chain using rigid Kuhn segments. At zero force, the FRC model predicts a contour length of $R_0 = N l_e \cos(\phi_e/2)$ and a mean-square end-to-end distance of $\langle r^2 \rangle = N l_e^2 (1 + \cos \phi_e) / (1 - \cos \phi_e)$, giving the equivalent Kuhn length in the FJC* model $l_k = \langle r^2 \rangle / R_0 = 2 l_e \cos(\phi_e/2) / (1 - \cos \phi_e)$ [21]. As shown in Fig. 3, all models agree well with experimental data at low forces ($r/R_0 \leq 0.8$), where the response is entropy-dominated. At intermediate forces ($0.8 < r/R_0 \leq 0.9$), the FRC model outperforms the FJC* model by incorporating fixed bond angles, better capturing the effect of angular constraints on chain configurations. However, at high forces ($r/R_0 > 0.9$), the FRC model diverges from experimental data as bond deformations start to dominate the response. In contrast, our statistical model remains accurate across the entire force range by capturing these energetic effects. Both bond stretching and bond angle opening contribute significantly to the response, as reflected in the dimensionless bond parameters $k_l l_e^2 / k_B T = 2466$ and $k_\phi \pi^2 / k_B T = 1810$, which strongly influence chain stiffness at high forces (Fig. 2).

The statistical model provides an exact force-extension relationship for given potential energies (up to numerical error) but does not have a closed-form expression and thus cannot readily be incorporated into micromechanical models. To address this, we develop a semi-analytical estimate that remains valid across the entire force range and also predicts bond stretch, which is important for future modeling of polymer failure by chain scission. Following the approach proposed by Lavoie et al. [18], we consider the Helmholtz free energy Ψ of a polymer chain under a prescribed end-to-end distance r . This free energy is approximated by assuming uniform and fixed (non-fluctuating) bond length and bond angle:

$$\Psi = N v_{str}(l) + (N - 1) v_{ben}(\phi) + \Psi_{ent}(r, l, \phi) \quad (7)$$

where the first two terms respectively represent the energetic contributions due to bond stretching and bond angle deformation, and the third term Ψ_{ent} is the entropic contribution. In Ref. [18], Ψ_{ent} was obtained by integrating the closed-form force-extension relation of the WLC model, where the persistence length was expressed in terms of bond length and bond angle. However, this WLC representation introduces additional approximations which are difficult to quantify. Here, in contrast,

we directly take Ψ_{ent} as the free energy of a FRC with bond length l and bond angle ϕ , consistent with the decomposition in Eq. 7. The bond parameters l and ϕ are determined by minimizing the Helmholtz free energy at a prescribed chain end-to-end distance r , which implies $(\partial\Psi/\partial l)_{r,\phi} = (\partial\Psi/\partial\phi)_{r,l} = 0$. The force-displacement response is then derived as $f = d\Psi/dr = (\partial\Psi_{ent}/\partial r)_{l,\phi}$. We call our model “deformable FRC” (dFRC).

To simplify model implementation, a fully analytical expression for the FRC free energy, valid across the entire force range, is needed. Existing formulations are either limited to specific force ranges or require fitting parameters [8, 20]. To address this, we propose a new analytical formula for the force-extension relation of a FRC:

$$f = \frac{k_B T}{l_k} \left\{ \beta + \frac{1}{2} \frac{(r^*)^2}{(1-r^*)^2} \left[1 - (r^*)^{l_k/l-1} \right] \right\} \quad (8)$$

where $\beta = \mathcal{L}^{-1}(r^*)$ and $\mathcal{L}(x) = \coth(x) - 1/x$ is the Langevin function. Here, $r^* = r/R_{max}$ represents the relative end-to-end distance, with the contour length given by $R_{max} = Nl \cos(\phi/2)$. The equivalent Kuhn length is $l_k = \langle r^2 \rangle / R_{max} = 2l \cos(\phi/2) / (1 - \cos\phi)$, where the mean-square end-to-end distance is $\langle r^2 \rangle = Nl^2(1 + \cos\phi) / (1 - \cos\phi)$. The free energy $\Psi_{ent}(r, l, \phi)$ can then be obtained by integrating the force-extension relationship as: $\Psi_{ent}(r, l, \phi) = \int f dr$, giving:

$$\Psi_{ent} = k_B T \frac{R_{max}}{l_k} \left[r^* \beta + \ln \frac{\beta}{\sinh \beta} + \frac{1 + r^*(1-r^*)}{2(1-r^*)} + \ln(1-r^*) - \frac{1}{2} \mathcal{B}(r^*; 2 + l_k/l, -1) \right] \quad (9)$$

where $\mathcal{B}(x; a, b) = \int_0^x t^{a-1} (1-t)^{b-1} dt$ is the incomplete beta function. Note that when the bonds are freely jointed, only bond stretching is considered, with the bond length l determined by energy minimization. In this case, the Kuhn length and mean-square end-to-end distance are $l_k = l$ and $R_{max} = Nl$, respectively. The force-extension relationship (Eq. 8) recovers the FJC model with $f = (k_B T / l_k) \beta$, and the entropic energy (Eq. 9) becomes $\Psi_{ent}(r, l) = Nk_B T \left[r^* \beta + \ln \frac{\beta}{\sinh \beta} \right]$. The Helmholtz free energy (Eq. 7) reduces to $\Psi = Nv_{str}(l) + \Psi_{ent}(r, l)$, corresponding to the semi-analytical extensible FJC model proposed by Mao et al. [15].

We verify the accuracy of the analytical FRC formula (Eq. 8) by comparing its predictions to reference numerical results obtained using the statistical model (TM) across a wide range of bond angles ($\phi = 10^\circ - 90^\circ$) (Fig. 4). Eq. 8 shows a remarkable agreement with TM, maintaining a relative error below 6% over the entire force range ($fl_e/k_B T = 10^{-3.5} - 10^{2.5}$). To the best of our knowledge, this is the first global analytical formula for the FRC model that is entirely free of fitting parameters.

We next validate the semi-analytical dFRC model for a polymer chain with extensible bonds and deformable

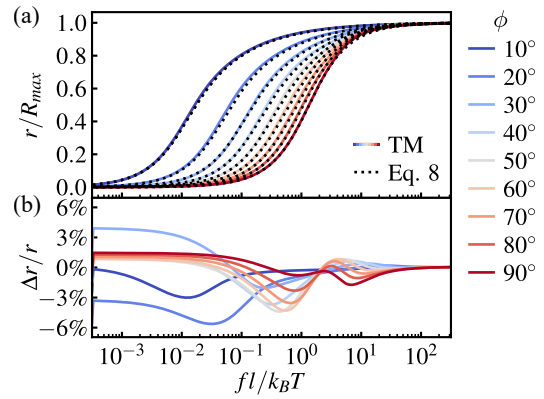


FIG. 4. Comparison of the statistical model (TM) and the proposed analytical formula (Eq. 8) for a FRC with fixed bond length l and bond angle ϕ . (a) Force-extension curves. (b) Relative error of Eq. 8 compared to TM.

bond angles by comparing its predicted force-extension relationships to reference results from the statistical model (TM). Additionally, we investigate the validity of the model core assumption of uniform bond length and bond angle, see also Sec. S5. The semi-analytical extensible FJC model is similarly validated against the statistical model in Sec. S5.1. Here, we consider two representative cases:

(i) Extensible bonds and fixed bond angles ($k_\phi \pi^2 / k_B T \rightarrow \infty$). The Helmholtz free energy (Eq. 7) reduces to $\Psi = Nv_{str}(l) + \Psi_{ent}(r, l, \phi_e)$. In the force-extension relation (Eq. 8), l is determined by energy minimization, while the bond angle is fixed at $\phi = \phi_e$. The bond length distribution $P_i^l(l)$ given by the statistical model varies for the first few bonds but quickly converges to a stable distribution $P_\infty^l(l)$ with increasing bond index i . This distribution depends on the bond stretching stiffness k_l (which controls the length variance) and the applied force f (which shifts the average bond length) (Sec. S5.2). As shown in Fig. 5b, for $k_l l_e^2 / k_B T = 10^3$, $P_\infty^l(l)$ remains concentrated around its most probable value, supporting the uniform bond length assumption. The optimized bond length in the dFRC model closely follows the peak of $P_\infty^l(l)$, yielding an accurate force-extension prediction (Fig. 5a). Even for $k_l l_e^2 / k_B T = 10^1$, where bond length is more widely distributed, the dFRC model still approximates the force-extension response well (Fig. S13).

(ii) Rigid bonds ($k_l l_e^2 / k_B T \rightarrow \infty$) and deformable bond angles. The Helmholtz free energy (Eq. 7) reduces to $\Psi = (N-1)v_{ben}(\phi) + \Psi_{ent}(r, l_e, \phi)$. In the force-extension relation (Eq. 8), the bond angle ϕ is determined by energy minimization, while the bond length is fixed at $l = l_e$. With increasing bond index i , the bond angle distribution $P_i^\phi(\phi)$ given by the statistical model quickly stabilizes to $P_\infty^\phi(\phi)$, which is shaped by the bond angle deformation stiffness k_ϕ and the applied force f (Sec.

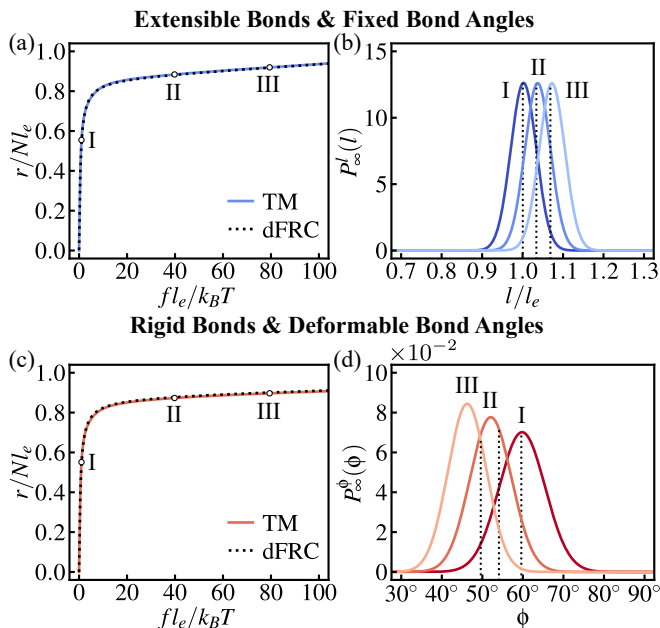


FIG. 5. Comparison of statistical (TM) and semi-analytical (dFRC) models for chains with deformable bonds. (a) Force-extension curve for a chain with extensible bonds ($k_l l_e^2 / k_B T = 10^3$) and fixed bond angles ($k_\phi \pi^2 / k_B T = 10^3$, $\phi_e = 60^\circ$). (b) Converged bond length distribution in the statistical model at different forces from (a). (c) Force-extension curve for a chain with rigid bonds ($k_l l_e^2 / k_B T \rightarrow \infty$) and deformable bond angles ($k_\phi \pi^2 / k_B T = 10^3$, $\phi_e = 60^\circ$). (d) Corresponding converged bond angle distribution from (c). In (b) and (d), black dotted lines indicate the optimized bond lengths or angles in the dFRC model.

S5.3). For $k_\phi \pi^2 / k_B T = 10^3$, $P_\infty^\phi(\phi)$ is narrowly distributed, supporting the uniform bond angle assumption (Fig. 5d). As f increases, $P_\infty^\phi(\phi)$ narrows further and shifts to the left, indicating a reduction in both the average bond angle and its variability. At lower applied forces, the optimized bond angle in the dFRC model aligns closely with the peak of $P_\infty^\phi(\phi)$, corresponding to the most probable bond angle. However, at higher forces, the optimized value exceeds the peak of $P_\infty^\phi(\phi)$ (Fig. 5d). This discrepancy arises from approximation errors in the proposed FRC formula (Eq. 9), which increase at smaller bond angles. Consequently, the dFRC model loses precision in predicting bond angles at high forces. Nevertheless, it accurately predicts the force-extension relation (Fig. 5c). The accuracy of the dFRC model also depends on k_ϕ . As k_ϕ decreases, the bond angle distribution broadens, and the dFRC model performance deteriorates, becoming inapplicable for $k_\phi \pi^2 / k_B T = 10$ (Fig. S17).

Finally, we apply the dFRC model to carbon chains, using the same parameters as in Fig. 3, taken from [22]. As shown in Fig. 6a, the dFRC model closely reproduces the force-extension behavior of the statistical model (TM). We also examine the evolution of the

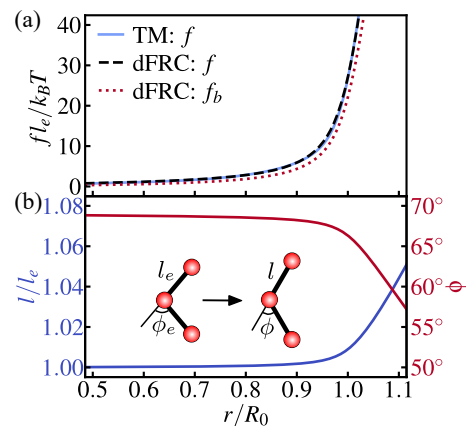


FIG. 6. Application of the dFRC model to carbon chains. (a) Chain force f predicted by the statistical (TM) and dFRC models, along with bond force f_b from the dFRC model. (b) Evolution of bond length l and bond angle ϕ in the dFRC model.

bond length and bond angle with the applied stretch predicted by the dFRC model (Fig. 6b). When the extension ratio is below $r/R_0 \leq 0.9$, the response is entropy-dominated, with bond lengths and angles remaining at their equilibrium values. This explains why the force-extension curve in this regime aligns with that of the classical FRC model (Fig. 3). For larger extension ratios, energetic contributions become significant, leading to bond stretching and bond angle opening. Based on the predicted bond length, we obtain the bond force as $f_b = \partial v_{str}(l) / \partial l = k_l(l - l_e)$, which is a key factor in determining chain scission [23–25]. As shown in Fig. 6a, in the initial entropy-dominated regime, f_b is almost zero due to negligible bond stretching. As bond deformation becomes significant, f_b increases but always remains lower than the chain force f , because the chain deformation is influenced by both bond stretching and bond angle opening, reducing the direct force on individual bonds. We also compare the prediction of the extensible FJC model [15] with experimental data [9] for carbon chains and find that using physical parameters fails to reproduce the correct force-extension curve (Sec. S6). This highlights the necessity of incorporating both bond stretching and bond angle opening in chain elasticity models.

In summary, we have developed a statistical and a semi-analytical (dFRC) model to describe the stretching behavior of polymer chains, incorporating both bond stretching and bond angle opening for accurate predictions at large deformations. Both models are applied to carbon chains using molecular mechanics-derived parameters and show excellent agreement with experimental data across all force regimes. The dFRC model is suited for integration into micromechanical models to improve predictions of network elasticity and failure. While we adopted quadratic bond stretching and bond angle opening energies, our formulations are not restricted

to these choices and can accommodate other potential forms, such as Lennard-Jones or Morse potentials. Future work could extend these models to hybrid chains with multiple backbone bond types, less flexible chains with large side groups and strong rotation hindrance, and rate-dependent deformation and failure.

The authors thank Lucas Mangas Araujo from University of Oxford and Kangjie Zheng from Peking University for important discussions and helpful comments on the manuscript. J.Z. acknowledges the support of an EPSRC DTP studentship at the University of Oxford. L.B. acknowledges supports from UKRI through a Future Leaders Fellowship [MR/W006995/1].

-
- [1] L. G. Treloar, *The physics of rubber elasticity* (Oxford University Press, 1975).
- [2] M. C. Wang and E. Guth, Statistical theory of networks of non-gaussian flexible chains, *The Journal of Chemical Physics* **20**, 1144 (1952).
- [3] E. M. Arruda and M. C. Boyce, A three-dimensional constitutive model for the large stretch behavior of rubber elastic materials, *Journal of the Mechanics and Physics of Solids* **41**, 389 (1993).
- [4] P. Wu and E. Van Der Giessen, On improved network models for rubber elasticity and their applications to orientation hardening in glassy polymers, *Journal of the Mechanics and Physics of Solids* **41**, 427 (1993).
- [5] L. M. Araujo, I. Kryven, and L. Brassart, Micromechanical modelling of rubbery networks: The role of chain pre-stretch, *International Journal of Non-Linear Mechanics* **166**, 104834 (2024).
- [6] G. Kumar and L. Brassart, On tube models of rubber elasticity: fitting performance in relation to sensitivity to the invariant I_2 , *Mechanics of Soft Materials* **5**, 6 (2023).
- [7] P. J. Flory and M. Volkenstein, *Statistical mechanics of chain molecules* (Wiley Online Library, 1969).
- [8] T. Hugel, M. Rief, M. Seitz, H. E. Gaub, and R. R. Netz, Highly stretched single polymers: Atomic-force-microscope experiments versus ab-initio theory, *Physical Review Letters* **94**, 048301 (2005).
- [9] K. Wang, X. Pang, and S. Cui, Inherent stretching elasticity of a single polymer chain with a carbon-carbon backbone, *Langmuir* **29**, 4315 (2013).
- [10] S. Lu, W. Cai, N. Cao, H. Qian, Z. Lu, and S. Cui, Understanding the extraordinary flexibility of polydimethylsiloxane through single-molecule mechanics, *ACS Materials Letters* **4**, 329 (2022).
- [11] N. Balabaev and T. Khazanovich, Extension of chains composed of freely joined elastic segments, *Russian Journal of Physical Chemistry B* **3**, 242 (2009).
- [12] F. Manca, S. Giordano, P. L. Palla, R. Zucca, F. Cleri, and L. Colombo, Elasticity of flexible and semiflexible polymers with extensible bonds in the Gibbs and Helmholtz ensembles, *The Journal of Chemical Physics* **136** (2012).
- [13] A. Fiasconaro and F. Falo, Analytical results of the extensible freely jointed chain model, *Physica A: Statistical Mechanics and its Applications* **532**, 121929 (2019).
- [14] M. R. Buche, M. N. Silberstein, and S. J. Grutzik, Freely jointed chain models with extensible links, *Physical Review E* **106**, 024502 (2022).
- [15] Y. Mao, B. Talamini, and L. Anand, Rupture of polymers by chain scission, *Extreme Mechanics Letters* **13**, 17 (2017).
- [16] A. Fiasconaro and F. Falo, Elastic traits of the extensible discrete wormlike chain model, *Physical Review E* **107**, 024501 (2023).
- [17] R. R. Netz, Strongly stretched semiflexible extensible polyelectrolytes and DNA, *Macromolecules* **34**, 7522 (2001).
- [18] S. R. Lavoie, R. Long, and T. Tang, Modeling the mechanics of polymer chains with deformable and active bonds, *The Journal of Physical Chemistry B* **124**, 253 (2019).
- [19] R. J. Baxter, *Exactly solved models in statistical mechanics* (Elsevier, 2016).
- [20] L. Livadaru, R. Netz, and H. Kreuzer, Stretching response of discrete semiflexible polymers, *Macromolecules* **36**, 3732 (2003).
- [21] M. Rubinstein and R. H. Colby, *Polymer physics* (Oxford University Press, 2003).
- [22] R. Sorensen, W. Liao, L. Kesner, and R. Boyd, Prediction of polymer crystal structures and properties: polyethylene and poly (oxymethylene), *Macromolecules* **21**, 200 (1988).
- [23] S. Wang, S. Panyukov, M. Rubinstein, and S. L. Craig, Quantitative adjustment to the molecular energy parameter in the Lake-Thomas theory of polymer fracture energy, *Macromolecules* **52**, 2772 (2019).
- [24] B. Deng, S. Wang, C. Hartquist, and X. Zhao, Nonlocal intrinsic fracture energy of polymerlike networks, *Physical Review Letters* **131**, 228102 (2023).
- [25] Q. Guo and F. Zaïri, A micromechanics-based model for deformation-induced damage and failure in elastomeric media, *International Journal of Plasticity* **140**, 102976 (2021).
- [26] S. M. Ross, *Introduction to probability models* (Academic press, 2014).
- [27] B. Talamini, Y. Mao, and L. Anand, Progressive damage and rupture in polymers, *Journal of the Mechanics and Physics of Solids* **111**, 434 (2018).
- [28] B. Li and N. Bouklas, A variational phase-field model for brittle fracture in polydisperse elastomer networks, *International Journal of Solids and Structures* **182**, 193 (2020).
- [29] J. Mulderrig, B. Li, and N. Bouklas, Affine and non-affine microsphere models for chain scission in polydisperse elastomer networks, *Mechanics of Materials* **160**, 103857 (2021).
- [30] P. K. Arunachala, S. A. Vajari, M. Neuner, and C. Linder, A multiscale phase field fracture approach based on the non-affine microsphere model for rubber-like materials, *Computer Methods in Applied Mechanics and Engineering* **410**, 115982 (2023).

Supplementary Material: Stretching Response of a Polymer Chain with Deformable Bonds

Jie Zhu¹ and Laurence Brassart¹

¹*Department of Engineering Science,
University of Oxford, Oxford OX1 3PJ, United Kingdom.*

arXiv:2502.08602v1 [cond-mat.soft] 12 Feb 2025

S1 THEORETICAL FRAMEWORK OF THE STATISTICAL MODEL

Consider a polymer chain consisting of $N + 1$ atoms connected by N bonds (Fig. 1). In the Gibbs ensemble, the first atom is fixed at position $\vec{r}_0 = (0, 0, 0)$, and the last atom is subjected to a prescribed force \vec{f} . The chain configuration is described by the atom positions \vec{r}_i ($i = 1, \dots, N$) and momenta \vec{p}_i ($i = 1, \dots, N$). The dynamics of the system is described by the augmented Hamiltonian:

$$\tilde{h}(\vec{r}_1, \dots, \vec{r}_N, \vec{p}_1, \dots, \vec{p}_N, \vec{f}) = T(\vec{p}_1, \dots, \vec{p}_N) + V(\vec{r}_1, \dots, \vec{r}_N) - \vec{f} \cdot \vec{r}_N \quad (\text{S1})$$

where $T(\vec{p}_1, \dots, \vec{p}_N) = \sum_{i=1}^N [\vec{p}_i \cdot \vec{p}_i / (2m)]$ is the kinetic energy with m the mass of an atom, $V(\vec{r}_1, \dots, \vec{r}_N)$ is the interaction energy of the atoms, and $-\vec{f} \cdot \vec{r}_N$ is the potential energy of the applied force.

In thermal equilibrium with a reservoir at temperature T , the chain properties are described by the canonical ensemble distribution:

$$\rho(q, p; \vec{f}, T) = \frac{1}{Z} e^{-\frac{\tilde{h}(q, p, \vec{f})}{k_B T}} \quad (\text{S2})$$

where $q \equiv (\vec{r}_1, \dots, \vec{r}_N)$, $p \equiv (\vec{p}_1, \dots, \vec{p}_N)$, k_B is the Boltzmann constant, and Z is the canonical partition function in the Gibbs ensemble:

$$Z(\vec{f}, T) = \iint e^{-\frac{\tilde{h}(q, p, \vec{f})}{k_B T}} dq dp = (2\pi m k_B T)^{3N/2} \int e^{-\frac{1}{k_B T} [V(q) - \vec{f} \cdot \vec{r}_N]} dq \quad (\text{S3})$$

where we have integrated over the momenta. Since $\partial \tilde{h} / \partial \vec{f} = -\vec{r}_N$, the mean position of the last atom is given by $\vec{r} = \langle \vec{r}_N \rangle = -\langle \partial \tilde{h} / \partial \vec{f} \rangle$, where $\langle \cdot \rangle \equiv \iint \cdot dq dp$. Alternatively, the force-extension relation can directly be obtained from the partition function as [S1]:

$$\vec{r}(\vec{f}, T) = k_B T \frac{\partial}{\partial \vec{f}} \ln Z = -\frac{\partial G(\vec{f}, T)}{\partial \vec{f}} \quad (\text{S4})$$

where $G(\vec{f}, T) = -k_B T \ln Z$ is the Gibbs free energy of the chain.

For further analysis, we introduce the bond vectors $\vec{l}_i = \vec{r}_i - \vec{r}_{i-1}$ ($i = 1, \dots, N$) and represent them in spherical coordinates, $\vec{l}_i = l_i (\sin \theta_i \cos \varphi_i, \sin \theta_i \sin \varphi_i, \cos \theta_i)$, as shown in Fig. 1. Here, l_i is the length of i th bond, $\theta_i \in [0, \pi]$ is the polar angle with respect to the direction of applied force \vec{f} , and $\varphi_i \in [0, 2\pi)$ is the azimuthal angle. The bond angle between the i th and $(i - 1)$ th bonds can be expressed as:

$$\phi_i = \angle(\vec{l}_{i-1}, \vec{l}_i) = \arccos[\sin \theta_i \sin \theta_{i-1} \cos \omega_i + \cos \theta_i \cos \theta_{i-1}] \quad (\text{S5})$$

where $\omega_i = \varphi_i - \varphi_{i-1}$ is the difference in azimuthal angle between these two bonds. The interaction potential of the atoms is taken as:

$$V = \sum_{i=1}^N v_{str}(l_i) + \sum_{i=2}^N v_{ben}(\phi_i) \quad (\text{S6})$$

where $v_{str}(l)$ is the energy for stretching the bond between two adjacent atoms, and $v_{ben}(\phi)$ is the energy for deforming the angle between two consecutive bonds. In this work, we adopt the simple quadratic expressions: $v_{str}(l) = \frac{1}{2}k_l(l - l_e)^2$ and $v_{ben}(\phi) = \frac{1}{2}k_\phi(\phi - \phi_e)^2$, where l_e and ϕ_e are the equilibrium bond length and bond angle, respectively. k_l and k_ϕ are the stiffness for bond extension and bond angle deformation, respectively. Throughout this work, we do not consider the torsional energy of the bonds, i.e. we assume that bonds can freely rotate. The partition function becomes:

$$Z(f, T) = (2\pi m k_B T)^{3N/2} \int e^{-\frac{1}{k_B T} [\sum_{i=1}^N v_{str}(l_i) + \sum_{i=2}^N v_{ben}(\phi_i) - \sum_{i=1}^N f l_i \cos \theta_i]} dq' \quad (\text{S7})$$

where $q' \equiv (\vec{l}_1, \dots, \vec{l}_N)$ and $f = \|\vec{f}\|$.

S2 TRANSFER-MATRIX TECHNIQUE

S2.1 General solution

Direct calculation of the partition function (Eq. S7) is challenging due to the dependence of the interaction potential on the bond angle ϕ , which introduces a coupling between the orientations of two consecutive bonds. To address this difficulty, we adopt the transfer-matrix (TM) technique [S2], inspiring from Ref. [S3]. The partition function is rewritten in the equivalent form:

$$Z(f, T) = (2\pi m k_B T)^{3N/2} \int B_N(\theta) d\theta \quad (\text{S8})$$

where the function $B_i(\theta)$ ($i = 1, \dots, N$) measures the probability of finding the i th bond at a certain angle θ with respect to the direction of the applied force. It is obtained via the recursive formula:

$$B_{i+1}(\theta) = \int B_i(\theta') T(\theta, \theta') d\theta' \quad (\text{S9})$$

with the initial distribution

$$B_1(\theta) = 2\pi \int e^{-\frac{1}{k_B T} [v_{str}(l) - f l \cos \theta]} l^2 \sin \theta dl \quad (\text{S10})$$

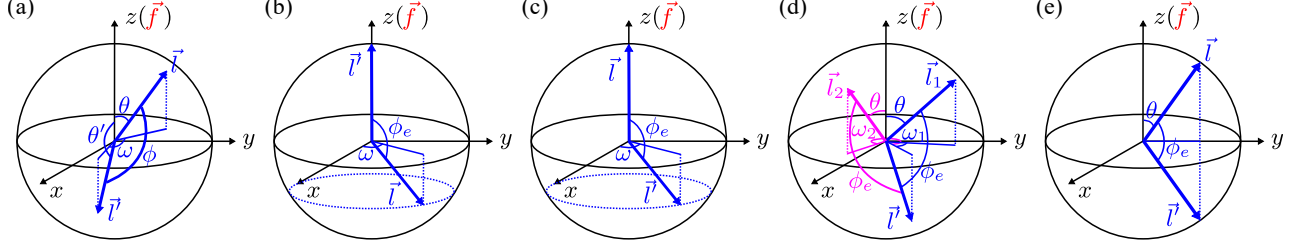


FIG. S1. Spherical coordinates used in the transfer-matrix schemes for (a) a deformable bond angle ϕ and (b-e) a fixed bond angle ϕ_e . (b) $\theta' = 0$, $\theta = \phi_e$, and ω can be any value in the range of $[0, 2\pi)$. (c) $\theta = 0$, $\theta' = \phi_e$, and ω can be any value in the range of $[0, 2\pi)$. (d) $|\cos \omega| < 1$, and ω has two possible values. (e) $\omega = 0$, and $\theta' = \theta + \phi_e$.

$T(\theta, \theta')$ is the transfer operator describing the interactions between two consecutive bonds at angles θ and θ' . It is given by:

$$T(\theta, \theta') = \iint e^{-\frac{1}{k_B T} [v_{str}(l) + v_{ben}(\phi) - fl \cos \theta]} l^2 \sin \theta d\omega dl \quad (\text{S11})$$

where $\phi = \arccos [\sin \theta \sin \theta' \cos \omega + \cos \theta \cos \theta']$ and ω is the difference in azimuthal angle between these two bonds (Fig. S1a). Mathematically, Eq. S9 resembles a Chapman-Kolmogorov equation, with $T(\theta, \theta')$ serving as a conditional probability density [S4]. Starting from $B_1(\theta)$, the $B_i(\theta)$ of each subsequent bonds can be computed iteratively, and the partition function can be obtained from Eq. S8.

To keep the high-dimensional integration within a numerically manageable range, it is convenient to define the rescaled function:

$$W_{i+1}(\theta) = \frac{B_{i+1}(\theta)}{\int B_i(\theta') d\theta'} \quad (\text{S12})$$

For the first bond, $W_1(\theta) = B_1(\theta)$. Substituting Eq. S9 into Eq. S12 gives:

$$W_{i+1}(\theta) = \int P_i(\theta') T(\theta, \theta') d\theta' \quad (\text{S13})$$

where $P_i(\theta)$ is the probability density of finding the i th bond at an angle θ :

$$P_i(\theta) = \frac{B_i(\theta)}{\int B_i(\theta') d\theta'} = \frac{W_i(\theta)}{\int W_i(\theta') d\theta'} \quad (\text{S14})$$

It is clear that $\int P_i(\theta) d\theta = 1$. The original probability function $B_{i+1}(\theta)$ can then be expressed as:

$$B_{i+1}(\theta) = W_{i+1}(\theta) \prod_{j=1}^i \left[\int W_j(\theta) d\theta \right] \quad (\text{S15})$$

and the partition function (Eq. S8) becomes:

$$Z(f, T) = (2\pi m k_B T)^{3N/2} \prod_{i=1}^N \left[\int W_i(\theta) d\theta \right] \quad (\text{S16})$$

Finally, the Gibbs free energy can be expressed as:

$$G(f, T) = -k_B T \sum_{i=1}^N \ln \left[\int W_i(\theta) d\theta \right] \quad (\text{S17})$$

up to an additive constant independent of f . The force-extension relation of the chain is given as:

$$r(f, T) = -\frac{\partial G(f, T)}{\partial f} \quad (\text{S18})$$

where $r = \|\vec{r}\|$ is the chain end-to-end distance.

In practice, the functions $W_{i+1}(\theta)$ are calculated iteratively via the probabilities $P_i(\theta)$ using Eqs S13 and S14, starting from $W_1(\theta) = B_1(\theta)$, Eq. S10. The integral in the transfer operator, Eq. S11, is computed numerically by discretizing the length range of l uniformly into M_l intervals, and the angular range of ω uniformly into M_ω intervals. Next, the integrals in Eqs S13 and S14 are computed numerically by discretizing the angular range of θ uniformly into M_θ intervals. In the general case of deformable bond angles, we found that taking $M_\omega = 100$, $M_l = 50(l_{max} - l_{min})/l_e$ and $M_\theta = 50$ is sufficient to achieve convergence. Here l_{max} and l_{min} represent the maximum and minimum bond length used in the numerical calculation, set as $2l_e$ and 0, respectively. Note that increasing l_{max} can cause numerical overflow for large applied force (e.g. $fl_e/k_B T > 10^{2.5}$). Finally, the Gibbs free energy is calculated using Eq. S17, and the chain extension for a given force is calculated using Eq. S18, where the derivative is approximated by finite differences.

Fig. S2a shows the transfer operator $T(\theta, \theta')$ for rigid bonds ($k_l l_e^2/k_B T \rightarrow \infty$) and deformable bond angles ($\phi_e = 60^\circ$, $k_\phi \pi^2/k_B T = 10^4$). Because the Boltzmann factor $e^{-k_B T(\phi - \phi_e)^2}$ strongly favors $\phi \approx \phi_e$, $T(\theta, \theta')$ shows sharp peaks in regions where this condition is satisfied. For example, when $\theta = \phi_e$, $T(\theta, \theta')$ is sharply peaked near $\theta' = 0$, while at $\theta = \pi/2$, the peaks appear around $\theta' = \pi/2 \pm \phi_e$ (Fig. S2d). As k_ϕ increases, these peaks grow in magnitude. In addition, $T(\theta, \theta')$ is modulated by the geometric weighting $\sin \theta$, which reflects how orientations are distributed on the unit sphere. Near $\theta = 0$ or $\theta = \pi$, $\sin \theta$ is small, so even if the Boltzmann factor is large, its product with $\sin \theta$ remains small. Conversely, around $\theta = \pi/2$, $\sin \theta$ is the largest, favoring those configurations unless the bending energy strongly disfavors them.

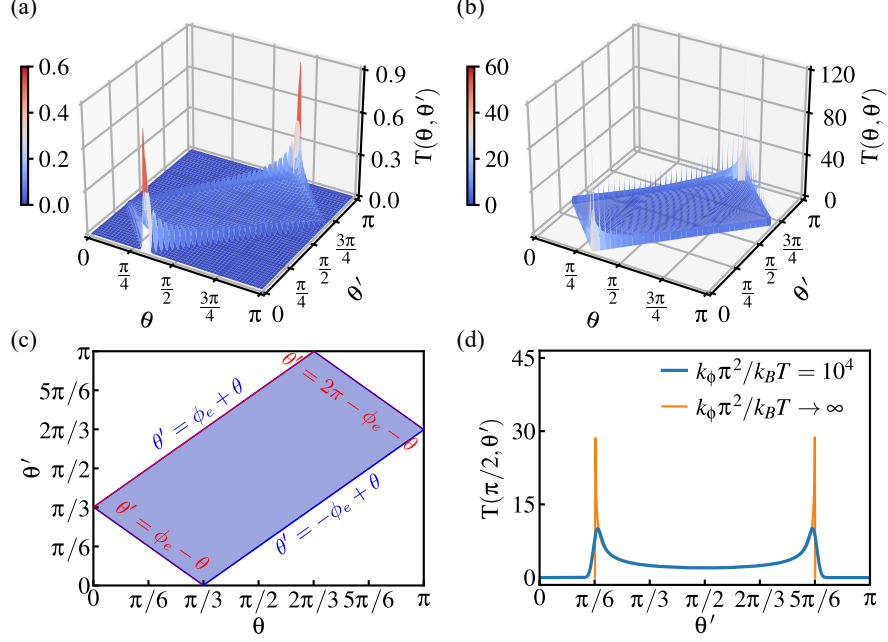


FIG. S2. Transfer operator $T(\theta, \theta')$ for (a) a deformable bond angle ($\phi_e = 60^\circ$, $k_\phi \pi^2 / k_B T = 10^4$) and (b) a fixed bond angle ($\phi_e = 60^\circ$, $k_\phi \pi^2 / k_B T \rightarrow \infty$). In both cases, the bonds are rigid, and no external force is applied. (c) shows the domain of the transfer operator in the case of fixed bond angle. (d) compares $T(\pi/2, \theta')$ for cases (a) and (b). In the deformable bond angle case, the Boltzmann factor $e^{-(k_\phi/2k_B T)(\phi - \phi_e)^2}$ equals 1 at $\phi = \phi_e$, while in the fixed bond angle case, the delta function $\delta(\phi - \phi_e)$ is infinite at $\phi = \phi_e$. To enable a direct comparison, the transfer operators are normalized by their integrals over ϕ , respectively given by $\int e^{-(k_\phi/2k_B T)(\phi - \phi_e)^2} d\phi = \sqrt{2\pi k_B T / k_\phi}$ and $\int \delta(\phi - \phi_e) d\phi = 1$.

S2.2 Limiting Case 1: Freely Jointed Bonds

When $k_\phi = 0$, the bonds are freely jointed, and the transfer operator (Eq. S11) simplifies to:

$$T(\theta) = 2\pi \int e^{-\frac{1}{k_B T} [v_{str}(l) - fl \cos \theta]} l^2 \sin \theta dl \quad (\text{S19})$$

Then, it is readily seen from Eqs S10 and S13 that $W_{i+1}(\theta) = W_1(\theta) = T(\theta)$. Consequently, the partition function becomes:

$$Z(f, T) \propto \left[2\pi \iint e^{-\frac{1}{k_B T} [v_{str}(l) - fl \cos \theta]} l^2 \sin \theta dl d\theta \right]^N \quad (\text{S20})$$

Integration over θ can be carried out analytically, giving:

$$Z(f, T) \propto \left[4\pi \int e^{-\frac{1}{k_B T} [v_{str}(l)]} \frac{\sinh(fl/k_B T)}{fl/k_B T} l^2 dl \right]^N \quad (\text{S21})$$

The chain end-to-end distance $r(f, T)$ is then expressed as:

$$r(f, T) = N k_B T \frac{\partial}{\partial f} \ln \left[\int e^{-\frac{1}{k_B T} [v_{str}(l)]} \frac{\sinh(fl/k_B T)}{fl/k_B T} l^2 dl \right] \quad (\text{S22})$$

These results agree with the findings in Ref. [S1].

When $k_l l_e^2 / k_B T \rightarrow \infty$, bonds are rigid with $l = l_e$. The classical Freely Jointed Chain (FJC) model is then recovered [S5]:

$$r(f, T) = N k_B T \frac{\partial}{\partial f} \ln \left[\frac{\sinh(fl_e/k_B T)}{fl_e/k_B T} \right] = N l_e \mathcal{L} \left(\frac{fl_e}{k_B T} \right) \quad (\text{S23})$$

where $\mathcal{L}(x) = \coth(x) - 1/x$ is the Langevin function.

S2.3 Limiting Case 2: Fixed Bond Angles

When $k_\phi \pi^2 / k_B T \rightarrow \infty$, the angle between two consecutive bonds is constant with $\phi = \phi_e$. The transfer operator (Eq. S11) becomes:

$$\mathbb{T}(\theta, \theta') = \iint e^{-\frac{1}{k_B T} [v_{str}(l) - fl \cos \theta]} \delta(\phi - \phi_e) l^2 \sin \theta d\omega dl \quad (\text{S24})$$

where $\phi = \arccos[\sin \theta \sin \theta' \cos \omega + \cos \theta \cos \theta']$. Using the Dirac delta function composition rule, for fixed θ and θ' , the delta function $\delta(\phi - \phi_e)$ can be expressed in terms of ω as:

$$\delta(\phi - \phi_e) = \sum_i \frac{\delta(\omega - \omega_i)}{|(d\phi/d\omega)_{\omega=\omega_i}|} \quad (\text{S25})$$

where ω_i are the roots of $\phi(\omega) - \phi_e = 0$. They satisfy

$$\sin \theta \sin \theta' \cos \omega + \cos \theta \cos \theta' - \cos \phi_e = 0 \quad (\text{S26})$$

Several cases should be discussed:

- (i) If $\sin \theta' = 0$ ($\theta' = 0$ or $\theta' = \pi$), ω can be any value in the range of $[0, 2\pi)$. According to Eq. S26, we have $\theta = \phi_e$ or $\theta = \pi - \phi_e$ depending on the value of θ' (Fig. S1b). The transfer operators corresponding to these two special cases are given by:

$$\mathbb{T}(\phi_e, 0) = 2\pi \int e^{-\frac{1}{k_B T} [v_{str}(l) - fl \cos \phi_e]} l^2 \sin \phi_e dl \quad (\text{S27})$$

and:

$$\mathrm{T}(\pi - \phi_e, \pi) = 2\pi \int e^{-\frac{1}{k_B T} [v_{str}(l) + fl \cos \phi_e]} l^2 \sin \phi_e dl \quad (\text{S28})$$

For other values of θ , we set $\mathrm{T}(\theta, 0) = 0$ and $\mathrm{T}(\theta, \pi) = 0$.

- (ii) If $\sin \theta = 0$ ($\theta = 0$ or $\theta = \pi$), ω can be any value in the range of $[0, 2\pi)$ and $\theta' = \phi_e$ or $\theta' = \pi - \phi_e$ (Fig. S1c). Then:

$$\mathrm{T}(0, \phi_e) = 0 \quad (\text{S29})$$

and:

$$\mathrm{T}(\pi, \pi - \phi_e) = 0 \quad (\text{S30})$$

- (iii) If $\sin \theta \sin \theta' \neq 0$, then ω should satisfy

$$\cos \omega = \frac{\cos \phi_e - \cos \theta \cos \theta'}{\sin \theta \sin \theta'} = g(\theta, \theta') \quad (\text{S31})$$

If $|g(\theta, \theta')| < 1$, there are two possible values of ω in the range of $[0, 2\pi)$: $\omega_1 = \arccos[g(\theta, \theta')]$ and $\omega_2 = 2\pi - \arccos[g(\theta, \theta')]$ (Fig. S1d). We also have:

$$\frac{d\phi}{d\omega} = \frac{\sin \theta \sin \theta' \sin \omega}{\sin \phi} \quad (\text{S32})$$

Then:

$$\left| \left(\frac{d\phi}{d\omega} \right)_{\omega=\omega_1} \right| = \left| \left(\frac{d\phi}{d\omega} \right)_{\omega=\omega_2} \right| = \frac{\sin \theta \sin \theta'}{\sin \phi_e} \sqrt{1 - \left(\frac{\cos \phi_e - \cos \theta \cos \theta'}{\sin \theta \sin \theta'} \right)^2} \quad (\text{S33})$$

The delta function $\delta(\phi - \phi_e)$ becomes

$$\delta(\phi - \phi_e) = \sum_{i=1}^2 \frac{\sin \phi_e}{\sqrt{(\sin \theta \sin \theta')^2 - (\cos \phi_e - \cos \theta \cos \theta')^2}} \delta(\omega - \omega_i) \quad (\text{S34})$$

Substituting it back to the transfer operator, we obtain:

$$\mathrm{T}(\theta, \theta') = \int e^{-\frac{1}{k_B T} [v_{str}(l) - fl \cos \theta]} \frac{2l^2 \sin \phi_e \sin \theta}{\sqrt{(\sin \theta \sin \theta')^2 - (\cos \phi_e - \cos \theta \cos \theta')^2}} dl \quad (\text{S35})$$

If $|g(\theta, \theta')| = 1$, ω also has two possible values: $\omega_1 = 0$ and $\omega_2 = \pi$ (Fig. S1e). At these points, $(d\phi/d\omega)_{\omega=\omega_1} = (d\phi/d\omega)_{\omega=\omega_2} = 0$, indicating a second-order zero of $\phi(\omega) - \phi_e$.

For a second-order zero at $\omega = \omega_i$, the delta function generalization is:

$$\delta(\phi - \phi_e) = \sum_{i=1}^2 \frac{\delta'(\omega - \omega_i)}{|(d^2\phi/d\omega^2)_{\omega=\omega_i}|/2} = \sum_{i=1}^2 \frac{2 \sin \phi_e \delta'(\omega - \omega_i)}{\sin \theta \sin \theta'} \quad (\text{S36})$$

and it immediately follows from the properties of the delta function derivative that $T(\theta, \theta') = 0$.

Finally, if $|g(\theta, \theta')| > 1$, there is no valid value of ω in the range of $[0, 2\pi)$, so $T(\theta, \theta') = 0$.

If in addition $k_l l_e^2 / k_B T \rightarrow \infty$ (rigid bonds), the Freely Rotating Chain (FRC) model is recovered. A statistical model for the FRC model was previously developed by Livadaru et al. [S3] using the TM technique. In their approach, the constraint of fixed bond angles was imposed by expressing the delta function $\delta(\phi - \phi_e)$ in terms of θ' and constructing the corresponding transfer operator to solve the probability function $B_i(\theta)$ for each bond.

The transfer operator $T(\theta, \theta')$ is non-zero only at specific points: $(\phi_e, 0)$ and $(\pi - \phi_e, \pi)$, or when the condition $|g(\theta, \theta')| < 1$ is satisfied. As a result, $T(\theta, \theta')$ exhibits discontinuities, as illustrated in Fig. S2b. Fig. S2c shows the domain of $T(\theta, \theta')$, highlighting discontinuities at $\theta' = \phi_e \pm \theta$, $\theta' = -\phi_e + \theta$, and $\theta' = 2\pi - \phi_e - \theta$. Fig. S2d compares the transfer operators in the cases of fixed bond angle ($\phi_e = 60^\circ$, $k_\phi \pi^2 / k_B T \rightarrow \infty$) and deformable bond angle ($\phi_e = 60^\circ$, $k_\phi \pi^2 / k_B T = 10^4$) when $\theta = \pi/2$. It is obvious that in fixed bond angle case, discontinuities appear at $\pi/2 \pm \phi_e$. Because of these discontinuities, the integral $\int P_i(\theta') T(\theta, \theta') d\theta'$ used in the computation of $W_{i+1}(\theta)$ must be handled with care. First, we identify the angles θ'_{r1} and θ'_{r2} where $|g(\theta, \theta')| = 1$ for each θ . We then discretize the angular range $(\theta'_{r1}, \theta'_{r2})$ uniformly into M_θ intervals, producing a set of points θ'_k . At each point θ'_k , $T(\theta, \theta'_k)$ is evaluated using Eq. S35, and $P_i(\theta'_k)$ is interpolated from $P_i(\theta)$. In this case, we find that taking $M_\theta = 250$ is sufficient to achieve convergence.

S3 BOND ORIENTATION PROBABILITIES

We examine the probabilities of bond orientation $P_i(\theta)$ (probability density of finding the i th bond at an angle θ) in several cases, highlighting the roles of the applied force f , bond stretching stiffness k_l , and bond angle deformation stiffness k_ϕ .

S3.1 Freely jointed bonds

In the freely jointed bond limit ($k_\phi = 0$, Sec. S2.2), all bond orientations have the same probability density, $P_i(\theta) = P(\theta)$. The applied force f biases $P(\theta)$ towards alignment with

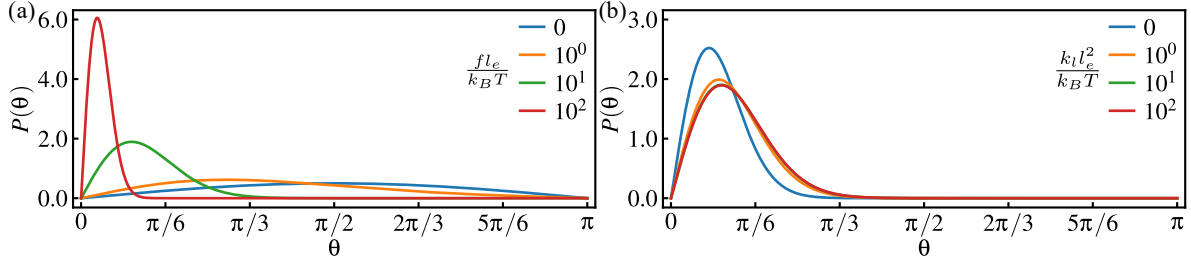


FIG. S3. Bond orientation probability density $P(\theta)$ for chains with freely jointed bonds. (a) Chains with rigid bonds ($k_l l_e^2 / k_B T \rightarrow \infty$) under applied forces $f l_e / k_B T = 0, 10^0, 10^1$, and 10^2 . (b) Chains with extensible bonds ($k_l l_e^2 / k_B T = 10^1, 10^2, 10^3$, and 10^4) under an applied force of $f l_e / k_B T = 10$.

the force direction ($\theta = 0^\circ$). Under no force, the bonds adopt random orientations, with $P(\theta) = \frac{1}{2} \sin \theta$ reflecting intrinsic geometric weighting (Fig. S3a). As f increases, $P(\theta)$ sharpens towards $\theta = 0^\circ$, indicating bond alignment in the force direction. Bond stretching, governed by k_l , further modulates this behavior. When k_l is small, the bond length l fluctuates significantly from l_e , broadening the integral over l in $W(\theta) = T(\theta)$, given by Eq. S19. The force term $-f l \cos \theta$ in the exponent favors longer bonds ($l > l_e$) when $\cos \theta > 0$ (i.e., for bonds aligned with the force). As a result, small k_l amplifies alignment, sharpening $P(\theta)$. In contrast, when k_l is large, the bond length remains nearly fixed at l_e , and only angular fluctuations contribute to the configurations, and $P(\theta)$ approaches the rigid bond limit (Fig. S3b).

S3.2 Fixed bond angles

In the fixed bond angle limit ($k_\phi \pi^2 / k_B T \rightarrow \infty$, Sec. S2.3), the coupling between the orientations of two successive bonds via the bending energy leads to distinct probability density functions $P_i(\theta)$ for each bond. The first bond, $P_1(\theta)$, behaves identically to the freely jointed case. As the bond index i increases, $P_i(\theta)$ converges to a stable distribution, $P_\infty(\theta)$ (Fig. S4). The applied force f influences both the convergence rate and the shape of $P_\infty(\theta)$. At small forces, $P_\infty(\theta)$ is similar to $P_1(\theta)$. As the applied force increases, $P_\infty(\theta)$ sharpens around $\phi_e/2$ and converges at higher index number (Fig. S4a). In the limit $f l_e / k_B T \rightarrow \infty$, the chain is fully straightened, and $P_\infty(\theta)$ collapses to a delta function, $\delta(\theta - \phi_e/2)$, corresponding to the all-*trans* (zig-zag) configuration. Bond stretching, controlled by k_l , affects $P_\infty(\theta)$ similar to the freely jointed case: a small k_l favors alignment, while a large k_l

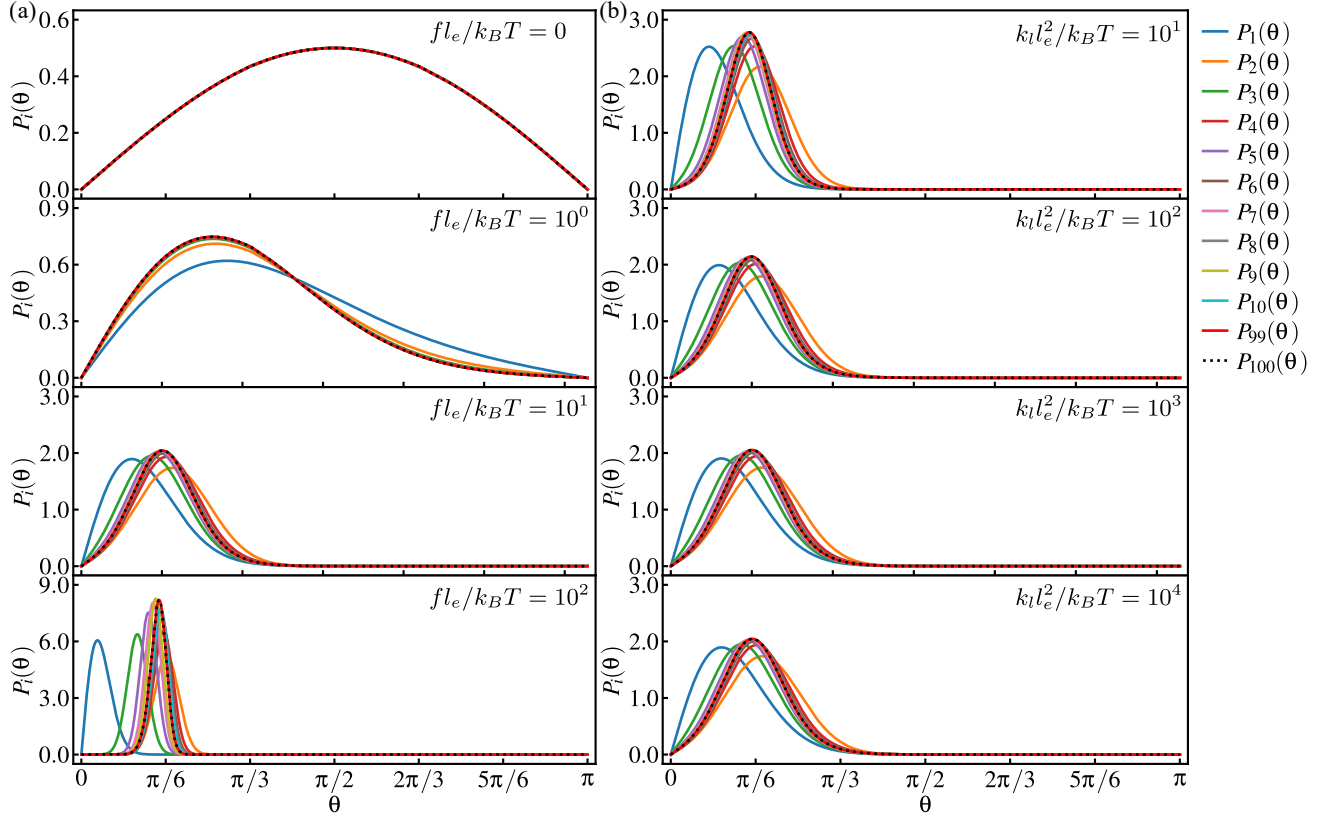


FIG. S4. Bond orientation probability density $P_i(\theta)$ for chains with a fixed bond angle $\phi_e = 60^\circ$. (a) Chains with rigid bonds ($k_l l_e^2 / k_B T \rightarrow \infty$) under applied forces $f l_e / k_B T = 0, 10^0, 10^1$, and 10^2 . (b) Chains with extensible bonds ($k_l l_e^2 / k_B T = 10^1, 10^2, 10^3$, and 10^4) under an applied force of $f l_e / k_B T = 10$.

hinders bond stretching, mimicking rigid bonds (Fig. S4b).

S3.3 Deformable bond angles

In the general case of deformable bond angles (Sec. S2.1), each bond exhibits a distinct orientation probability $P_i(\theta)$. The first bond, $P_1(\theta)$, behaves identically to the freely jointed case. For increasing bond index number i , $P_i(\theta)$ converges to a stable distribution, $P_\infty(\theta)$ (Fig. S5). Both the applied force f and the bond angle deformation stiffness k_ϕ affect the convergence rate and the shape of $P_\infty(\theta)$. At small forces, $P_\infty(\theta)$ remains similar to $P_1(\theta)$; at large forces, it sharpens around $\phi_e/2$, requiring more iterations to converge (Fig. S5a). The stiffness k_ϕ also plays a critical role: small k_ϕ allows easy bond angle deformation, making $P_\infty(\theta)$ similar to the freely jointed case, while large k_ϕ causes $P_i(\theta)$ to approach the fixed

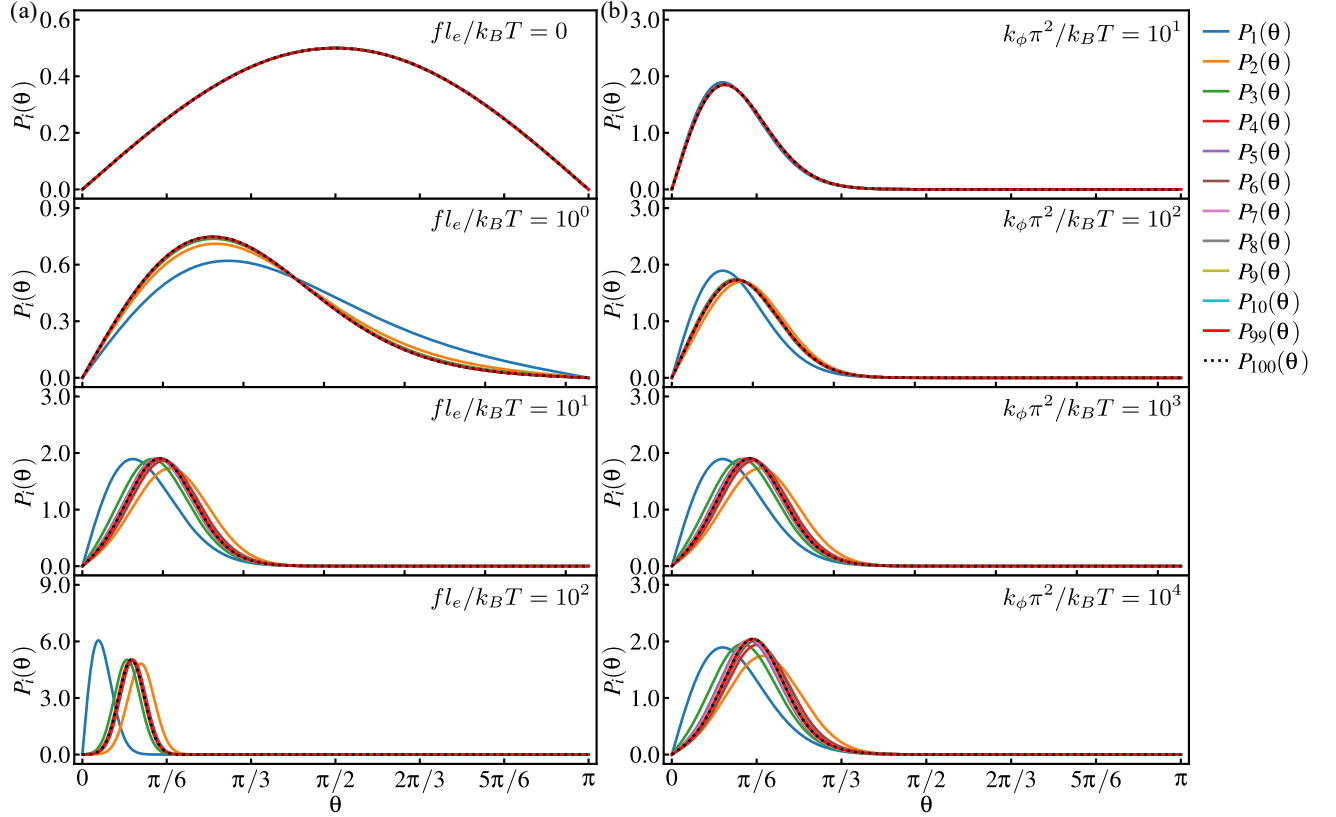


FIG. S5. Bond orientation probability density $P_i(\theta)$ for chains with rigid bonds ($k_l l_e^2/k_B T \rightarrow \infty$) and deformable bond angles ($\phi_e = 60^\circ$). (a) Chains with deformable bond angles ($k_\phi \pi^2/k_B T = 10^3$) under applied forces $fl_e/k_B T = 0, 10^0, 10^1$, and 10^2 . (b) Chain with deformable bond angles ($k_\phi \pi^2/k_B T = 10^1, 10^2, 10^3$, and 10^4) under an applied force of $fl_e/k_B T = 10$.

bond angle limit (Fig. S5b).

S4. FORCE-EXTENSION RELATIONSHIPS

S4.1 Effect of chain length

For freely jointed bonds ($k_\phi = 0$), the Gibbs partition function of a chain with N bonds can be expressed as the partition function of a single bond raised to the power N (Eq. S21). Consequently, the force-extension curve under prescribed force is independent of the chain length N , consistent with the findings in Ref. [S1].

When bond angles are constrained, the Gibbs partition function cannot be factorized, and the force-extension curve depends on N . However, for sufficiently large N ,

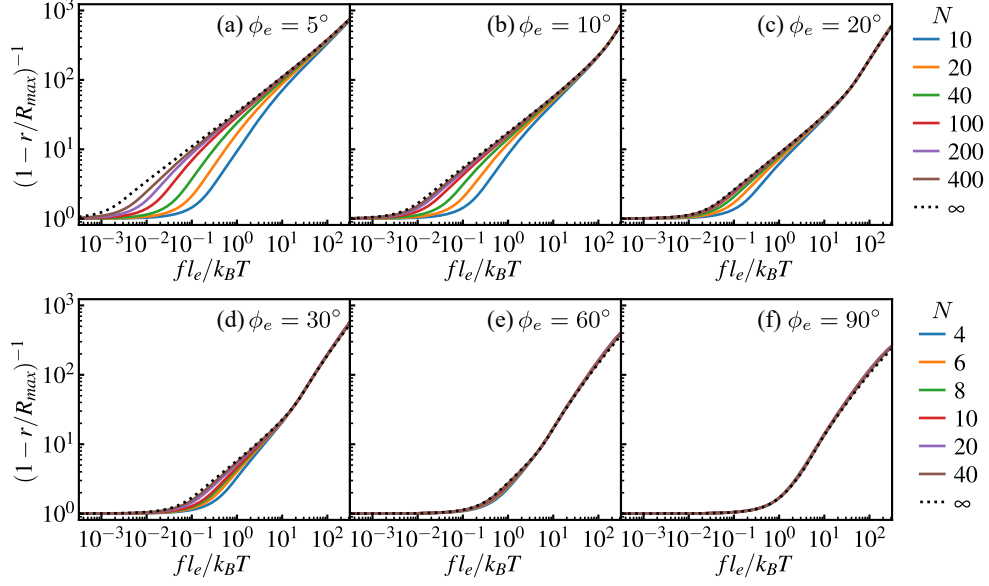


FIG. S6. Force-extension curves for chains with rigid bonds and fixed bond angles (FRC), showing dependence on chain length N for varying bond angles ϕ_e . (a) $\phi_e = 5^\circ$. (b) $\phi_e = 10^\circ$. (c) $\phi_e = 20^\circ$. (d) $\phi_e = 30^\circ$. (e) $\phi_e = 60^\circ$. (f) $\phi_e = 90^\circ$. Here R_{max} is the contour length of the chain, $R_{max} = Nl_e \cos(\phi_e/2)$.

the Gibbs partition function can be approximated as $Z \propto [\int W_\infty(\theta) d\theta]^N$, where $W_\infty(\theta) = \int P_\infty(\theta') T(\theta, \theta') d\theta'$. Here, $P_\infty(\theta)$ is the converged bond orientation probability. In this regime, the force-extension curve becomes independent on N , corresponding to the thermodynamic limit.

For chains with fixed bond angles at ϕ_e ($k_\phi \pi^2 / k_B T \rightarrow \infty$), the chain length N required to achieve this thermodynamic limit depends on ϕ_e . This is illustrated in Fig. S6 for a chain with rigid bonds (FRC). For large bond angles ($\phi_e \geq 30^\circ$), a small N ($N = 40$) is sufficient (Fig. S6d-f). However, for smaller bond angles ($\phi_e \rightarrow 0^\circ$), a larger N is needed to reach size independence (Fig. S6a-c). These results are consistent with the findings in Ref. [S3].

For chains with deformable bond angles, the effect of N on the force-extension curve is modulated by the bond angle deformation stiffness k_ϕ , as shown in Fig. S7 for a chain with rigid bonds and $\phi_e = 60^\circ$. When k_ϕ is small, the chain behaves similarly to the freely jointed case, with the force-extension curve nearly independent of N (Fig. S7a). As k_ϕ increases, bond angles stiffen, and geometrical constraints between adjacent bonds become more pronounced. This increases the dependence on N , requiring larger chain lengths to

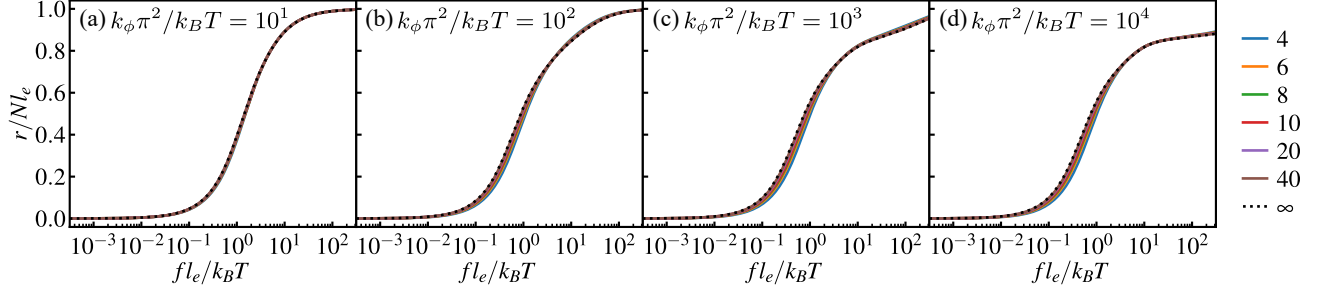


FIG. S7. Force-extension curves for chains with rigid bonds and deformable bond angles ($\phi_e = 60^\circ$), showing dependence on chain length N for varying bond angle deformation stiffness k_ϕ . (a) $k_\phi \pi^2 / k_B T = 10^1$. (b) $k_\phi \pi^2 / k_B T = 10^2$. (c) $k_\phi \pi^2 / k_B T = 10^3$. (d) $k_\phi \pi^2 / k_B T = 10^4$.

reach the thermodynamic limit (Fig. S7b-d).

S4.2 Effect of bond angle deformation

We examine the effect of bond angle deformation on the stretching response of chains with rigid bonds ($k_l l_e^2 / k_B T \rightarrow \infty$). The bond angle deformation stiffness k_ϕ governs the transition between the FJC and FRC models. When $k_\phi = 0$, the FJC model is recovered, and as $k_\phi \pi^2 / k_B T \rightarrow \infty$, the FRC model is recovered, with bond angles fixed at ϕ_e . Fig. S8 shows the force-extension behavior for varying stiffness k_ϕ and equilibrium angle ϕ_e . At low forces, the FRC model predicts a softer response compared to the FJC model. This occurs because the fixed bond angle in the FRC reduces the number of possible available conformations, favoring larger extensions under small force. At higher forces, however, this behavior reverses: the FRC model becomes stiffer because the fixed bond angles restrict the chain ability to extend. As the bonds align with the direction of the applied force, the FRC approaches its contour length, $R_{max} = Nl_e \cos(\phi_e/2)$. In contrast, the FJC, free from these angular constraints, can reach a larger contour length $R_{max} = Nl_e$. The equilibrium bond angle ϕ_e at a given k_ϕ also impacts the chain behavior, primarily by setting the contour length of the chain. In particular, for a FRC, the contour length ranges from $R_{max} = Nl_e / \sqrt{2}$ to $R_{max} = Nl_e$ (the FJC contour length) when ϕ_e goes from 90° to 0° .

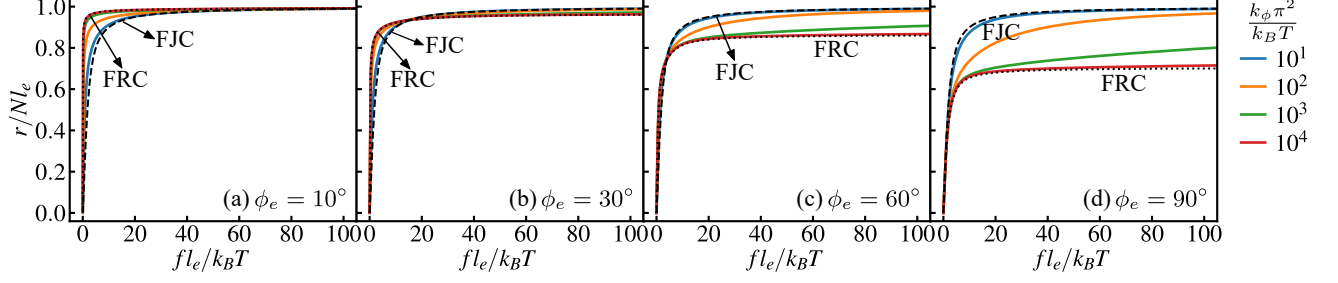


FIG. S8. Dependence of the force-extension curve on the bond angle deformation stiffness k_ϕ . The bonds are rigid ($k_l l_e^2/k_B T \rightarrow \infty$), with equilibrium bond angles of (a) $\phi_e = 10^\circ$, (b) $\phi_e = 30^\circ$, (c) $\phi_e = 60^\circ$, and (d) $\phi_e = 90^\circ$.

S5 VALIDATION OF THE SEMI-ANALYTICAL MODEL

The proposed semi-analytical dFRC model assumes that the behavior of a chain with fluctuating bond lengths and bond angles can be approximated by a FRC with uniformly fixed bond length and bond angle, determined such that they minimize the Helmholtz free energy of the chain at a prescribed chain stretch. In this section, we assess the validity of these assumptions by analyzing the probability distributions of bond length l and bond angle ϕ predicted by the statistical model and comparing their most probable values to those obtained using the semi-analytical model. Additionally, we validate the semi-analytical model by comparing predicted force-extension curves to reference curves obtained from the statistical model using TM method. Three representative cases are discussed.

S5.1 Freely jointed extensible bonds

We first consider the case of a chain with freely jointed bonds ($k_\phi = 0$). At an applied force f , the transfer operator simplifies to $T(\theta)$ (Eq. S19). In this scenario, all bonds have the same length probability distribution, $P^l(l)$, which is given by

$$P^l(l) = \frac{\int e^{-\frac{1}{k_B T} [v_{str}(l) - fl \cos \theta]} d\theta}{\iint e^{-\frac{1}{k_B T} [v_{str}(l) - fl \cos \theta]} d\theta dl} \quad (\text{S37})$$

The average bond length is

$$\langle l \rangle = \int l P^l(l) dl \quad (\text{S38})$$

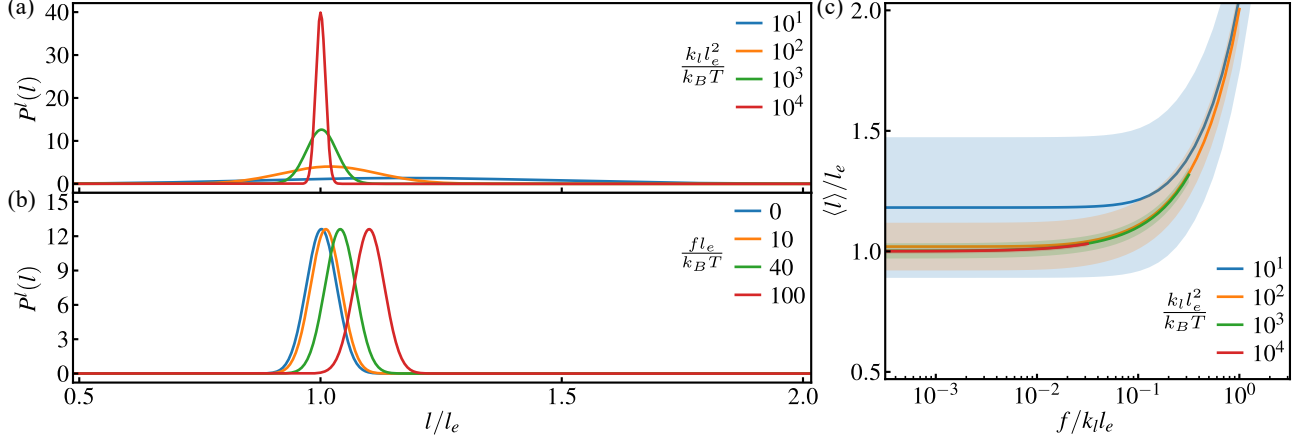


FIG. S9. Bond length probability distribution for a chain with freely jointed extensible bonds. (a) Bond length probability at zero applied force ($f = 0$) with varying bond stretching stiffness: $k_l l_e^2 / k_B T = 10^1, 10^2, 10^3$, and 10^4 . (b) Bond length probability for a fixed bond stretching stiffness $k_l l_e^2 / k_B T = 10^3$, under different applied forces: $f l_e / k_B T = 0, 10, 40$, and 100 . (c) Average bond length and standard deviation of the bond length as a function of $f / k_l l_e$.

and the corresponding variance is

$$\sigma_l^2 = \int (l - \langle l \rangle)^2 P^l(l) dl \quad (\text{S39})$$

The bond length probability distribution $P^l(l)$ is affected by two key factors: the bond stretching stiffness k_l and the applied force f . The stiffness k_l controls the spread of the distribution. As k_l increases, $P^l(l)$ becomes more narrowly concentrated around its mean value, indicating reduced bond length variability (Fig. S9a). In the limit $k_l l_e^2 / k_B T \rightarrow \infty$, the bond length is fixed at l_e , and the probability distribution converges to a delta function, $P^l(l) = \delta(l - l_e)$. On the other hand, the applied force f primarily affects the average bond length. Increasing f shifts the peak of $P^l(l)$ to the right, leading to a higher average bond length (Fig. S9b). Fig. S9c illustrates the dependence of the average bond length $\langle l \rangle$ and the standard deviation σ_l on the dimensionless force $f / k_l l_e$, for varying bond stretching stiffness. As $f / k_l l_e$ increases, $\langle l \rangle$ increases while σ_l decreases.

In the semi-analytical model, for a FJC with fixed bond length l , the force-extension relationship is given by

$$f = \frac{k_B T}{l} \beta \quad (\text{S40})$$

where $\beta = \mathcal{L}^{-1}(r/Nl)$ is the inverse Langevin function. The bond length l is determined by

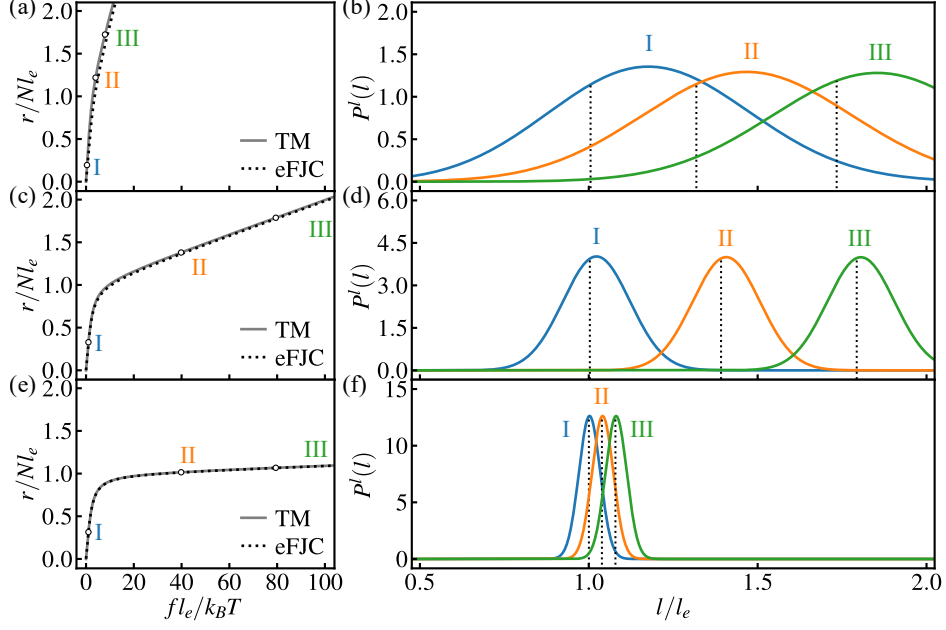


FIG. S10. Comparison of statistical (TM) and eFJC models for chains with freely jointed extensible bonds. (a), (c), and (e): Force-extension curves for bond stretching stiffness: $kl_e^2/k_B T = 10^1$, 10^2 , and 10^3 , respectively. (b), (d), and (f): Corresponding bond length distributions in the statistical model at different applied forces, where the black dotted lines represent the corresponding optimized bond lengths in the eFJC model.

minimizing the Helmholtz free energy of the chain at a prescribed chain end-to-end distance r . The Helmholtz free energy is expressed as

$$\Psi = Nv_{str}(l) + Nk_B T \left[\frac{r\beta}{Nl} + \ln \left(\frac{\beta}{\sinh \beta} \right) \right] \quad (\text{S41})$$

This extensible FJC (eFJC) model was first proposed by Mao et al. [S6], who used a logarithmic strain-based stretching energy $v_{str}(l) = \frac{1}{2}k_l[\ln(l/l_e)]^2$. The simpler quadratic form $v_{str}(l) = \frac{1}{2}k_l(l-l_e)^2$ was considered in their subsequent work [S7]. To enhance computational efficiency, Li and Bouklas proposed an approximate solution for l using the roots of cubic equations via trigonometric functions [S8]. Although this model has been widely used in the multiscale modeling of polymer fracture [S9–S11], the assumption of a uniformly fixed bond length has not been validated, nor have its force-extension predictions been compared to reference predictions obtained from the statistical mechanics model, leaving its accuracy uncertain.

We evaluate the accuracy of the eFJC model by comparing its predictions to numerical

results from the statistical model using the TM technique. Notably, even at a relatively low bond stretching stiffness ($k_l l_e^2/k_B T = 10^1$), the eFJC model provides a good approximation of the chain force-extension response (Fig. S10a), despite the broad bond length distribution deviating significantly from the uniform bond length assumption (Fig. S10b). As $k_l l_e^2/k_B T$ increases, the accuracy of the eFJC model increases. For $k_l l_e^2/k_B T = 10^3$, it accurately reproduces the chain stretching behavior (Fig. S10e), and the optimized bond length aligns with the most probable bond length in the bond length probability distribution calculated in the statistical model (Fig. S10f).

S5.2 Extensible bonds and fixed bond angles

We next consider the case of a chain with extensible bonds and fixed bond angles ($k_\phi \pi^2/k_B T \rightarrow \infty$) (extensible FRC). The transfer operator becomes (Sec. S2.3)

$$\mathbb{T}(\theta, \theta') = \begin{cases} 2\pi \sin \theta \int e^{-\frac{1}{k_B T} [v_{str}(l) - fl \cos \theta]} l^2 dl & (\theta, \theta') = (\phi_e, 0) \text{ or } (\pi - \phi_e, \pi) \\ 0 & (\theta, \theta') = (0, \phi_e) \text{ or } (\pi, \pi - \phi_e) \\ \frac{2 \sin \phi_e \sin \theta}{\sqrt{(\sin \theta \sin \theta')^2 - (\cos \phi_e - \cos \theta \cos \theta')^2}} \int e^{-\frac{1}{k_B T} [v_{str}(l) - fl \cos \theta]} l^2 dl & \sin \theta \sin \theta' \neq 0 \text{ and } |g(\theta, \theta')| < 1 \\ 0 & \sin \theta \sin \theta' \neq 0 \text{ and } |g(\theta, \theta')| \geq 1 \end{cases} \quad (\text{S42})$$

where $g(\theta, \theta') = (\cos \phi_e - \cos \theta \cos \theta')/\sin \theta \sin \theta'$, Eq. S31. Now consider the transfer operator before the integration with respect to l :

$$\mathbb{T}^l(\theta, \theta') = \begin{cases} 2\pi \sin \theta e^{-\frac{1}{k_B T} [v_{str}(l) - fl \cos \theta]} l^2 & (\theta, \theta') = (\phi_e, 0) \text{ or } (\pi - \phi_e, \pi) \\ 0 & (\theta, \theta') = (0, \phi_e) \text{ or } (\pi, \pi - \phi_e) \\ \frac{2 \sin \phi_e \sin \theta}{\sqrt{(\sin \theta \sin \theta')^2 - (\cos \phi_e - \cos \theta \cos \theta')^2}} e^{-\frac{1}{k_B T} [v_{str}(l) - fl \cos \theta]} l^2 & \sin \theta \sin \theta' \neq 0 \text{ and } |g(\theta, \theta')| < 1 \\ 0 & \sin \theta \sin \theta' \neq 0 \text{ and } |g(\theta, \theta')| \geq 1 \end{cases} \quad (\text{S43})$$

Under an applied force f , the bond length probability distribution of the $(i+1)$ th bond, $P_{i+1}^l(l)$, is given by

$$P_{i+1}^l(l) = \frac{\iint P_i(\theta') \mathbb{T}^l(\theta, \theta') d\theta' d\theta}{\iiint P_i(\theta') \mathbb{T}^l(\theta, \theta') d\theta' d\theta dl} \quad (\text{S44})$$

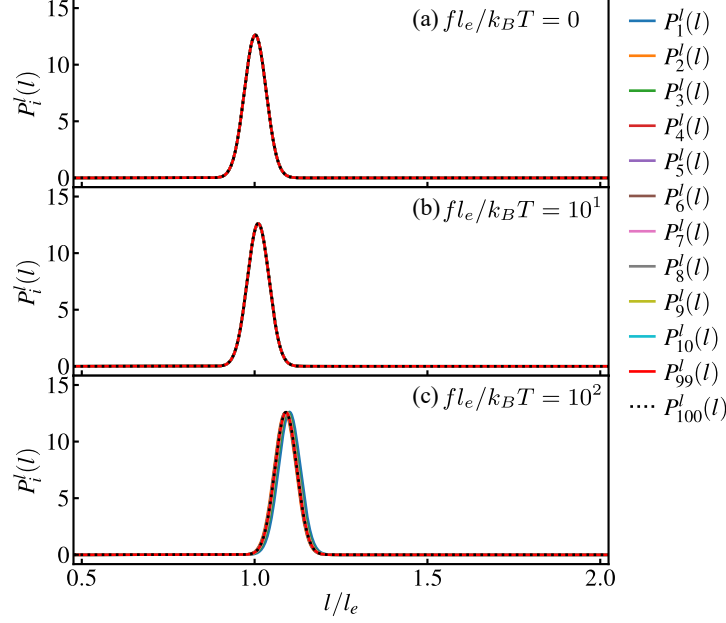


FIG. S11. Bond length probability density $P_i^l(l)$ for chains with extensible bonds ($k_l l_e^2 / k_B T = 10^3$) and a fixed bond angle of $\phi_e = 60^\circ$, subjected to applied forces (a) $f l_e / k_B T = 0$, (b) $f l_e / k_B T = 10^1$, and (c) $f l_e / k_B T = 10^2$.

recalling that $P_i(\theta)$ represents the bond orientation probability distribution of the i th bond. The bond length probability distribution of the 1st bond is

$$P_1^l(l) = \frac{\int e^{-\frac{1}{k_B T} [v_{str}(l) - f l \cos \theta]} l^2 \sin \theta d\theta}{\iint e^{-\frac{1}{k_B T} [v_{str}(l) - f l \cos \theta]} l^2 \sin \theta d\theta dl} \quad (\text{S45})$$

As shown in Fig. S11a, at zero force, all bonds have the same bond length probability distribution $P_i^l(l)$. As the force increases, $P_i^l(l)$ varies from bond to bond but converges to a steady-state distribution $P_\infty^l(l)$ as the bond index i increases. Although higher applied forces require a larger bond index to achieve convergence, the process remains relatively fast (Fig. S11c). Therefore, the converged distribution is a suitable representation of the bond length probability distribution in the chain. In the following analysis, we focus on examining the mean and variance of the converged bond length probability distribution for different parameters. The average bond length is

$$\langle l \rangle = \int l P_\infty^l(l) dl \quad (\text{S46})$$

and the corresponding variance is

$$\sigma_l^2 = \int (l - \langle l \rangle)^2 P_\infty^l(l) dl \quad (\text{S47})$$

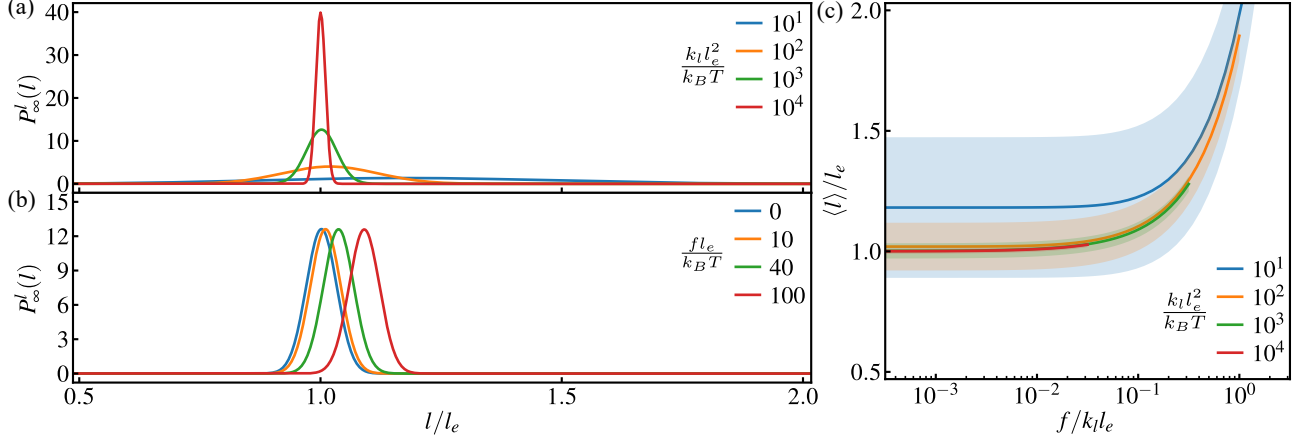


FIG. S12. Converged bond length probability distribution for a chain with extensible bonds and a fixed bond angle of $\phi_e = 60^\circ$. (a) Probability distributions at zero applied force ($f = 0$) for bond stretching stiffness: $k_l l_e^2 / k_B T = 10^1, 10^2, 10^3$, and 10^4 . (b) Probability distributions for a fixed bond stretching stiffness $k_l l_e^2 / k_B T = 10^3$ under different applied forces: $f l_e / k_B T = 0, 10, 40$, and 100 . (c) Average bond length and standard deviation as a function of $f / k_l l_e$.

The probability distribution $P_\infty^l(l)$ for fixed bond angles exhibits similar trends to the freely jointed bonds case. The bond stretching stiffness k_l controls the spread of the distribution, with higher k_l values leading to a narrower distribution centered around the average bond length (Fig. S12a). In the limit $k_l l_e^2 / k_B T \rightarrow \infty$, the distribution approaches $\delta(l - l_e)$. The applied force f primarily affects the average bond length, with increasing f shifting the peak of $P_\infty^l(l)$ to higher average bond length (Fig. S12b). Fig. S12c shows that $\langle l \rangle$ increases and σ_l decreases as $f / k_l l_e$ increases, consistent with the freely jointed bonds case.

The comparison between the semi-analytical (dFRC) and statistical models for fixed bond angles also mirrors the freely jointed bonds case. At $k_l l_e^2 / k_B T = 10^1$, the dFRC model approximates the force-extension response well (Fig. S13a), although the bond length distribution deviates from the uniform bond length assumption (Fig. S13b). As $k_l l_e^2 / k_B T$ increases, the semi-analytical model converges to the statistical model, achieving excellent agreement at $k_l l_e^2 / k_B T = 10^3$ (Fig. S13e). At this point, the optimized bond length in the dFRC model matches the most probable bond length in the distribution (Fig. S13f).

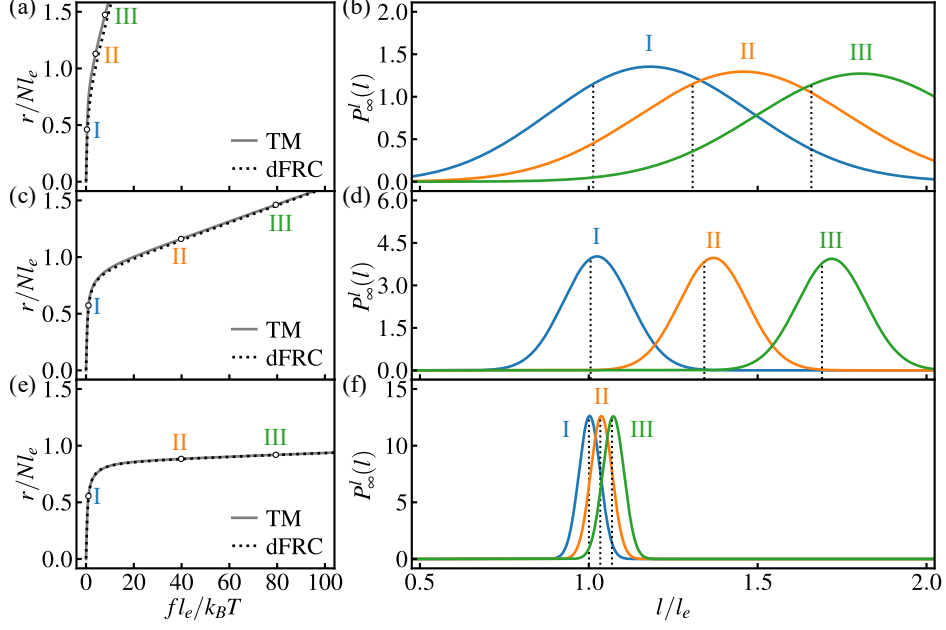


FIG. S13. Comparison of statistical (TM) and dFRC models for chains with extensible bonds and a fixed bond angle of $\phi_e = 60^\circ$. (a), (c), and (e): Force-extension curves for bond stretching stiffness $k_l l_e^2/k_B T = 10^1$, 10^2 , and 10^3 , respectively. (b), (d), and (f): Corresponding converged bond length distributions in the statistical model at different applied forces, where the black dotted lines represent the corresponding optimized bond lengths in the dFRC model.

S5.3 Rigid bonds and deformable bond angles

We next examine the bond angle probability distribution in a chain with rigid bonds ($k_l l_e^2/k_B T \rightarrow \infty$) and deformable bond angles. The transfer operator becomes

$$\mathbf{T}(\theta, \theta') = \int e^{-\frac{1}{k_B T} [v_{ben}(\phi) - f l_e \cos \theta]} \sin \theta d\omega \quad (\text{S48})$$

where θ and θ' are the polar angles of the $(i+1)$ th and i th bond orientations, respectively, measured relative to the direction of the applied force \vec{f} (Fig. S14a). The bond angle between these two bonds is given by $\phi = \arccos[\sin \theta \sin \theta' \cos \omega + \cos \theta \cos \theta']$, where ω is the difference in their azimuthal angle. The orientation probability distribution of the $(i+1)$ th bond is then given as $P_{i+1}(\theta) = \int P_i(\theta') \mathbf{T}(\theta, \theta') d\theta' / \iint P_i(\theta') \mathbf{T}(\theta, \theta') d\theta' d\theta$.

We now introduce the bond angle probability distribution $P_{i+1}^\phi(\phi)$, which is the probability of observing a bond angle ϕ between the i th and $(i+1)$ th bonds. To express everything in terms of ϕ (instead of θ), we rotate the coordinate system so that the new z -axis aligns with the i th bond \vec{l} (Fig. S14b). In this new frame, θ' and ϕ become the polar angles of the

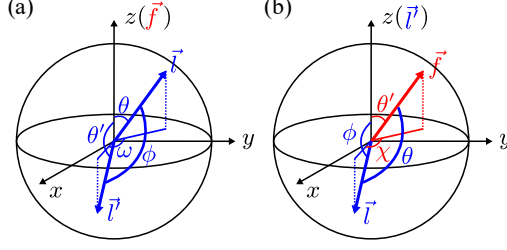


FIG. S14. Schematic representation of coordinates used in the calculation of (a) $P_i(\theta)$ and (b) $P_i^\phi(\phi)$.

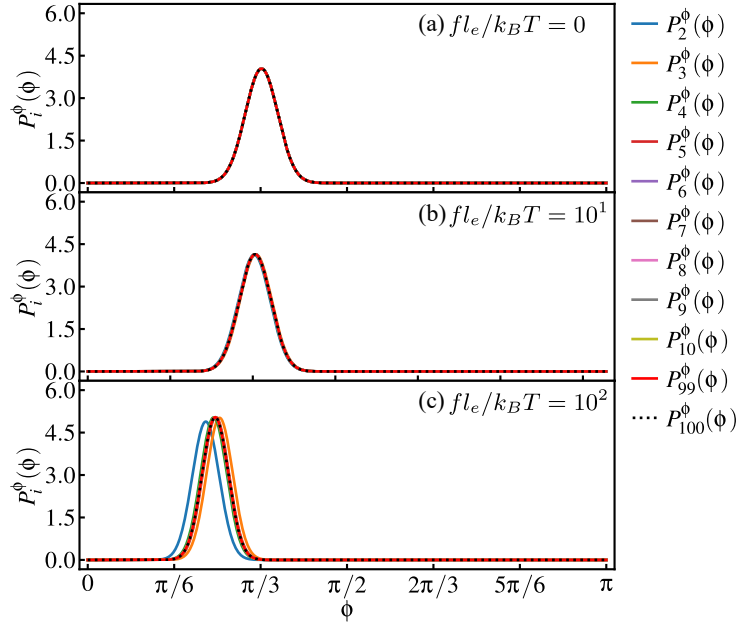


FIG. S15. Probability distribution of bond angles $P_i^\phi(\phi)$ for chains with rigid bonds and deformable bond angles ($\phi_e = 60^\circ$, $k_\phi \pi^2 / k_B T = 10^3$). The chains are subjected to applied forces (a) $fl_e/k_B T = 0$, (b) $fl_e/k_B T = 10^1$, and (c) $fl_e/k_B T = 10^2$.

applied force \vec{f} and the $(i+1)$ th bond \vec{l} relative to \vec{l}' , respectively. Then the angle between \vec{l} and \vec{f} , θ , can be expressed as $\theta = \arccos[\sin \theta' \sin \phi \cos \chi + \cos \theta' \cos \phi]$, where χ is the difference in azimuthal angles between \vec{f} and \vec{l} .

The bond angle probability distribution $P_{i+1}^\phi(\phi)$ is thus

$$P_{i+1}^\phi(\phi) = \frac{\iint P_i(\theta') e^{-\frac{1}{k_B T} [v_{ben}(\phi) - fl_e \cos \theta]} \sin \phi d\chi d\theta'}{\iiint P_i(\theta') e^{-\frac{1}{k_B T} [v_{ben}(\phi) - fl_e \cos \theta]} \sin \phi d\chi d\theta' d\phi} \quad (\text{S49})$$

Similar to the bond length probability distribution in the fixed bond angle case, the bond angle probability distribution $P_i^\phi(\phi)$ converges to a stable distribution $P_\infty^\phi(\phi)$ as the

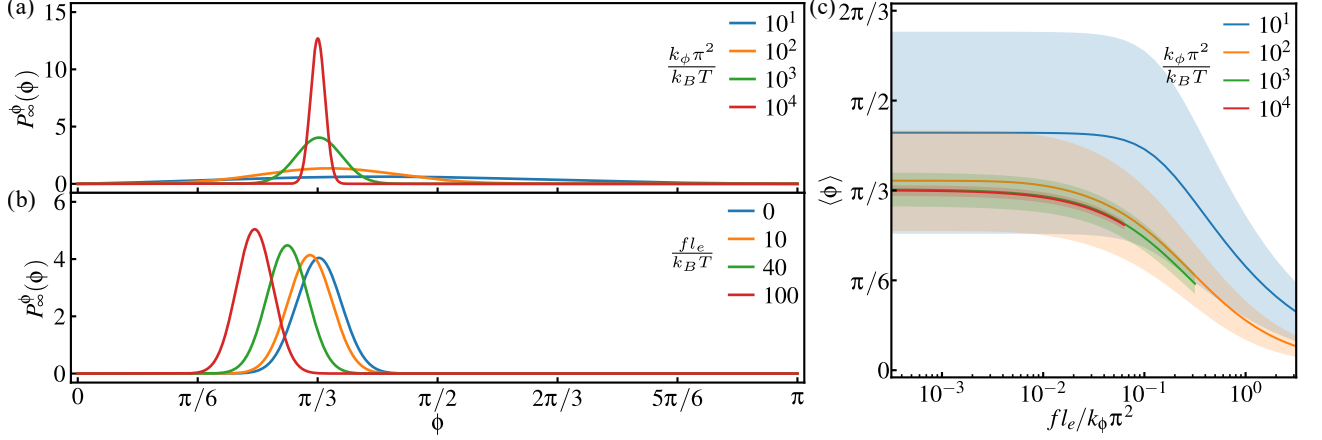


FIG. S16. Converged bond angle probability distribution in a chain with rigid bonds and deformable bond angles ($\phi_e = 60^\circ$). (a) Bond angle distribution at zero applied force ($f = 0$), with bond angle deformation stiffness: $k_\phi \pi^2/k_B T = 10^1, 10^2, 10^3$, and 10^4 . (b) Bond angle distribution with a fixed bond angle deformation stiffness of $k_\phi \pi^2/k_B T = 10^3$, subjected to applied forces: $f l_e/k_B T = 0, 10, 40$, and 100 . (c) Average bond angle and standard deviation as a function of $f l_e/k_\phi \pi^2$.

bond index i increases (Fig. S15). Higher applied forces require a larger bond index for convergence, but the process remains rapid. This converged distribution is used to represent the bond angle probability distribution, and we examine its mean and variance under varying parameters. The average bond angle is

$$\langle \phi \rangle = \int \phi P_\infty^\phi(\phi) d\phi \quad (\text{S50})$$

and the corresponding variance is

$$\sigma_\phi^2 = \int (\phi - \langle \phi \rangle)^2 P_\infty^\phi(\phi) d\phi \quad (\text{S51})$$

The converged bond angle distribution $P_\infty^\phi(\phi)$ depends on the bond angle deformation stiffness k_ϕ and the applied force f . The stiffness k_ϕ controls the spread of the distribution. As k_ϕ increases, $P_\infty^\phi(\phi)$ narrows around its mean value, indicating reduced bond angle variability (Fig. S16a). In the limit $k_\phi \pi^2/k_B T \rightarrow \infty$, the bond angle is fixed at ϕ_e , leading to $P_\infty^\phi(\phi) = \delta(\phi - \phi_e)$. Meanwhile, the applied force f primarily affects the average bond angle. Increasing f shifts the peak of $P_\infty^\phi(\phi)$ to the left, resulting in a lower average bond angle (Fig. S16b). Additionally, higher forces slightly sharpen the distribution, further reducing

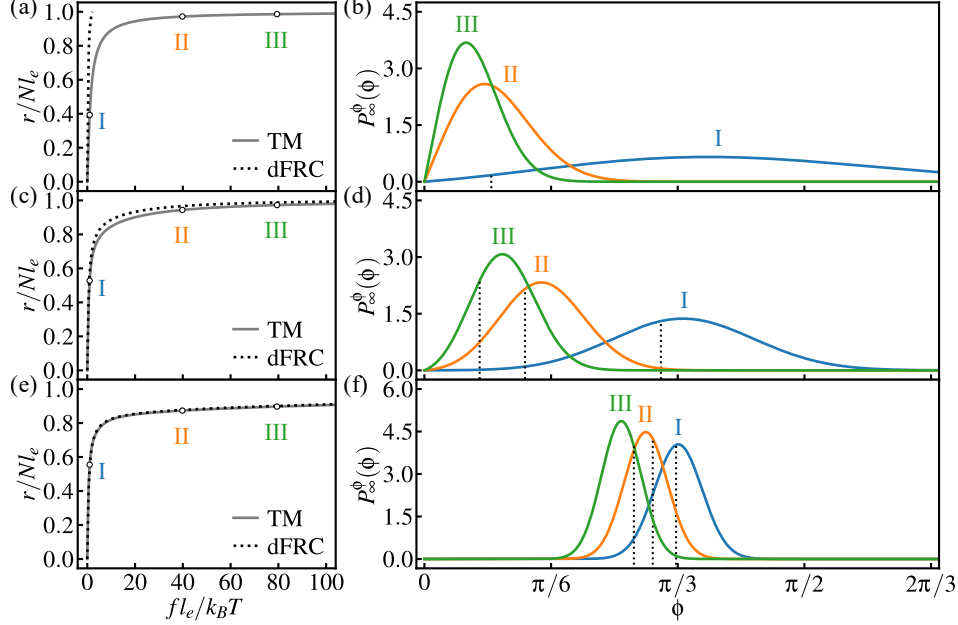


FIG. S17. Comparison of statistical (TM) and dFRC models for chains with rigid bonds and deformable bond angles ($\phi_e = 60^\circ$). (a), (c), and (e): Force-extension curves for the bond angle deformation stiffness $k_\phi\pi^2/k_B T = 10^1$, 10^2 , and 10^3 , respectively. (b), (d), and (f): Corresponding converged bond angle probability distributions in the statistical model at different applied forces, where the black dotted lines represent the corresponding optimized bond angles in the dFRC model.

bond angle variability. Fig. S16c illustrates the dependence of the average bond angle $\langle\phi\rangle$ and the standard deviation σ_ϕ on the dimensionless parameter $fl_e/k_\phi\pi^2$. As $fl_e/k_\phi\pi^2$ increases, both $\langle\phi\rangle$ and σ_ϕ decrease, highlighting the combined effect of f and k_ϕ on bond angle behavior.

Next, we compare how well the dFRC model captures bond angle deformation, using the predictions of the statistical model (TM) as reference. When the bond angle deformation stiffness is very small (eg. $k_\phi\pi^2/k_B T = 10^1$), the dFRC model deviates from the statistical model (Fig. S17a). This occurs because the bond angles are broadly distributed, making the uniform bond angle assumption in the dFRC model inapplicable (Fig. S17b). However, as $k_\phi\pi^2/k_B T$ increases, the bond angle distribution narrows, and the dFRC model increasingly aligns with the statistical model. At $k_\phi\pi^2/k_B T = 10^3$, it accurately reproduces the chain stretching response (Fig. S17e), although at high applied forces it predicts an optimized bond angle slightly larger than the distribution most probable value (Fig. S17f). For carbon chains, where the bond angle deformation stiffness can be as high as $k_\phi\pi^2/k_B T = 1810$, the

dFRC model can therefore reliably capture the effect of bond angle opening.

S6 APPLICATION OF THE EFJC TO CARBON CHAINS

As introduced in Sec. S5.1, the eFJC model proposed by Mao et al. has been widely adopted in polymer modeling. We have validated its accuracy against the statistical model for freely jointed extensible bonds, but its applicability to real polymer chains remains uncertain. Here, we apply the eFJC model to carbon chains, representing them as a series of extensible Kuhn segments. To differentiate this case from freely jointed extensible bonds, we refer to it as the eFJC* model. In the eFJC* model, the equilibrium Kuhn length is defined as $l_k = \langle r^2 \rangle / R_0 = 2l_e \cos(\phi_e/2)/(1 - \cos \phi_e)$, where $R_0 = Nl_e \cos(\phi_e/2)$ is the contour length and $\langle r^2 \rangle = Nl_e^2(1 + \cos \phi_e)/(1 - \cos \phi_e)$ is the mean-square end-to-end distance of the carbon chain at zero force. The stretching stiffness of Kuhn segment is assumed to match that of carbon-carbon bond [S6].

We compare predictions from the FJC* and eFJC* models with experimental data [S12] in Fig. S18a. Unlike the FJC* model, which exhibits a singularity at $r = R_0$ due to its rigid segment assumption, the eFJC* model allows chain extension beyond R_0 by incorporating extensible Kuhn segments. However, it still fails to capture the full stretching response of carbon chains, predicting a stiffer response than experimental data by neglecting bond angle deformation. In addition, we compare the chain force f and segment force $f_k = k_l(l_k - l_e)$, in Fig. S18b. At low forces ($r/R_0 < 0.75$), stretching is entropy-dominated, Kuhn segments remain nearly unstretched, and f_k is negligible. As the force increases, segments start to

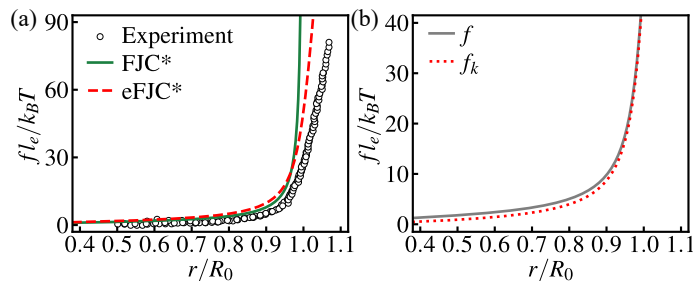


FIG. S18. Application of the eFJC* model to carbon chains. (a) Force-extension curves predicted by FJC* and eFJC* models, compared with experimental data from [S12]. (b) Chain force f and segment force f_k predicted by the eFJC* model. R_0 is the contour length at zero force.

stretch, leading to a rise in f_k . At high forces ($r/R > 0.95$), stretching becomes enthalpy-dominated, Kuhn segments align nearly linearly, and chain elongation results primarily from segment stretching, making f_k equal to f .

-
- [S1] F. Manca, S. Giordano, P. L. Palla, R. Zucca, F. Cleri, and L. Colombo, Elasticity of flexible and semiflexible polymers with extensible bonds in the Gibbs and Helmholtz ensembles, *The Journal of Chemical Physics* **136** (2012).
- [S2] R. J. Baxter, *Exactly solved models in statistical mechanics* (Elsevier, 2016).
- [S3] L. Livadaru, R. Netz, and H. Kreuzer, Stretching response of discrete semiflexible polymers, *Macromolecules* **36**, 3732 (2003).
- [S4] S. M. Ross, *Introduction to probability models* (Academic press, 2014).
- [S5] M. Rubinstein and R. H. Colby, *Polymer physics* (Oxford University Press, 2003).
- [S6] Y. Mao, B. Talamini, and L. Anand, Rupture of polymers by chain scission, *Extreme Mechanics Letters* **13**, 17 (2017).
- [S7] B. Talamini, Y. Mao, and L. Anand, Progressive damage and rupture in polymers, *Journal of the Mechanics and Physics of Solids* **111**, 434 (2018).
- [S8] B. Li and N. Bouklas, A variational phase-field model for brittle fracture in polydisperse elastomer networks, *International Journal of Solids and Structures* **182**, 193 (2020).
- [S9] J. Mulderrig, B. Li, and N. Bouklas, Affine and non-affine microsphere models for chain scission in polydisperse elastomer networks, *Mechanics of Materials* **160**, 103857 (2021).
- [S10] P. K. Arunachala, S. A. Vajari, M. Neuner, and C. Linder, A multiscale phase field fracture approach based on the non-affine microsphere model for rubber-like materials, *Computer Methods in Applied Mechanics and Engineering* **410**, 115982 (2023).
- [S11] P. K. Arunachala, S. Abrari Vajari, M. Neuner, J. S. Sim, R. Zhao, and C. Linder, A multiscale anisotropic polymer network model coupled with phase field fracture, *International Journal for Numerical Methods in Engineering* , e7488 (2024).
- [S12] K. Wang, X. Pang, and S. Cui, Inherent stretching elasticity of a single polymer chain with a carbon-carbon backbone, *Langmuir* **29**, 4315 (2013).